Die approbierte Originalversion dieser Dissertation ist an der Hauptbibliothek der Technischen Universität Wien aufgestellt (http://www.ub.tuwien.ac.at).

The approved original version of this thesis is available at the main library of the Vienna University of Technology (http://www.ub.tuwien.ac.at/englweb/).

DISSERTATION

Investigation of the Effects of Water and Temperature on the Adsorption of Alkylsiloxane Self-Assembled Monolayers on Silicon

ausgeführt zum Zwecke der Erlangung des akademischen Grades eines Doktors der technischen Wissenschaften unter der Leitung von

Ao. Univ.-Prof. Dipl.-Ing. Dr. techn. Gernot Friedbacher
Institut 164-IAC
Institut für Chemische Technologien und Analytik
der
Technischen Universität Wien

eingereicht an der Technischen Universität Wien
Fakultät für Technische Chemie

von

Dipl.-Ing. Andreas Glaser
Matrikelnummer 9225162
Sonnleithnergasse 57/3/26
1100 Wien

Wien, am 21. August 2005

1 Abstract / Kurzfassung

1.1 Abstract

Molecular self-assembly is an important phenomenon in nature. Spontaneous formation of organized monolayer films on various surfaces let alkylsilanes come to the fore in surface technology and analytics. The growth behavior of self-assembled monolayer films has been found to strongly depend on various parameters. In this work the adsorption of octadecyltrichlorosilane (OTS) from toluene was investigated with respect to the influence of the water concentration of the solvent and the deposition temperature. It has been found that growth kinetics, size, and shape of the obtained structures strongly depend on these parameters. The morphology of sub-monolayer films has been investigated by atomic force microscopy (AFM). The surface coverages have been determined both with ellipsometry and through quantitative evaluation of AFM images.

In order to obtain reproducible results, preparation of toluene with water concentrations in the lower mmol/L-range was necessary, which turned out to be non-trivial. Due to the temperature-dependent solubility of water in toluene stable stock solutions of water-saturated toluene cannot be prepared, and therefore the adjustment of the water content was alternatively achieved by direct doping with pure water. Optimization of this procedure was the basis for a series of deposition experiments, studying the influence of the water concentration on deposition kinetics and film structure. The thesis shows how the water content can be utilized to control the growth of self-assembled monolayer films.

The development of a temperature control unit was the basis for a further part of this work, studying the temperature as parameter for growth kinetics and resulting island structure. It has been found that octadecylsiloxane (ODS) island sizes decrease with increasing temperature. Secondly, a characteristic temperature exists, above which increasingly disordered growth takes place. At low temperatures (5 – 10°C) smaller dot-like features are observed besides larger fractally shaped islands characteristic for self-assembly growth of ODS films. The results indicate that these small circular features originate from ordered aggregates in the adsorption solution and that they are the precursors for the formation of larger islands. However,

they can only be observed at low temperatures, because at room temperature they coalesce quickly to larger units due to the high surface mobility.

Finally, the influence of the interplay of the temperature and the water concentration has been investigated. The size distribution of species in the precursor solution has been studied with dynamic light scattering which revealed a unimodal size distribution of ordered aggregates in solution with a hydrodynamic radius of 200 nm regardless of temperature and water concentration. However, formation of these features was faster at higher water contents and lower temperatures. Moreover, again a characteristic temperature – which was higher for higher water concentrations – was found above which such aggregates could not be detected anymore. Below this temperature a distinct increase of the aggregate concentration has been observed. Approximately 5°C below the characteristic temperature this increase finally ends in a plateau of constant aggregate concentration. AFM measurements and ellipsometry on the corresponding sub-monolayer films showed that this temperature range is also associated with a transition from slow homogeneous growth to fast island growth. The results are discussed in terms of diffusion- and adsorption-limitation of the deposition process.

Summarizing, it has been shown that the growth mechanism of ODS monolayers is strongly influenced by the temperature and the water concentration of the solvent and that these two parameters cannot be seen in an isolated manner. For each distinct water concentration the temperature decides whether diffusion or adsorption limited growth takes place and is also responsible for the occurrence of either ordered or homogenous growth. Moreover, the processes in the adsorption solution prior to the wafer immersion were found to very crucially influence the properties of the obtained films.

1.2 Kurzfassung

Molekulare Selbstorganisation ist ein wichtiges Phänomen in der Natur. Aufgrund der spontanen Bildung von organisierten Monolagen-Filmen auf verschiedenen Oberflächen rückten Alkylsilane ins Blickfeld der Oberflächentechnologie und der Analytik. Diverse Ergebnisse legten nahe, dass das Wachstumsverhalten von selbstorganisierten Filmen stark von verschiedenen Prozessparametern abhängt. Im Zuge dieser Arbeit wurde die Adsorption von Octadecyltrichlorsilan (OTS) aus Toluol hinsichtlich des Einflusses der Wasserkonzentration des Lösungsmittels und der Abscheidetemperatur untersucht. Es zeigte sich, dass die Wachstumskinetik sowie Größe und Form der gefundenen Strukturen stark von diesen beiden Parametern abhängt. Die Morphologie der Submonolagenfilme wurde mit der Rasterkraftmikroskopie (*atomic force microscopy* – AFM) untersucht. Die Ermittlung von Oberflächenbedeckungen erfolgte sowohl durch Ellipsometrie als auch durch quantitative Auswertung von AFM-Bildern.

Die reproduzierbare Herstellung von Toluol mit Wasserkonzentrationen im unteren mmol/L-Bereich, eine essentielle Voraussetzung für die angesprochenen Studien, erwies sich als schwierig, weil aufgrund der temperaturabhängigen Löslichkeit von Wasser in Toluol keine stabilen Stammlösungen von wassergesättigtem Toluol hergestellt werden konnten. Deshalb wurde der Wassergehalt durch direktes Dotieren mit reinem Wasser eingestellt. Die Optimierung dieses Verfahrens war die Grundlage für eine Serie von Adsorptionsexperimenten, bei denen der Einfluss der Wasserkonzentration auf die Abscheidekinetik und die Filmstruktur untersucht wurde. Diese Arbeit zeigt, wie der Wassergehalt verwendet werden kann, um das Wachstum von selbstorganisierten Monofilmen zu kontrollieren.

Die Entwicklung einer Temperaturregelung für die Abscheideversuche war die Voraussetzung für einen weiteren Teil dieser Arbeit, in dem die Temperatur als Parameter für die Wachstumskinetik und auftretende Inselstrukturen untersucht wurde. Es stellte sich heraus, dass die Octadecylsiloxan (ODS) - Inselgrößen mit zunehmender Temperatur kleiner wurden. Außerdem existiert eine charakteristische Temperatur, über der zunehmend ungeordnetes Wachstum stattfindet. Bei geringen Temperaturen (5 – 10°C) findet man neben den für das selbstorganisierte Wachstum

von ODS-Filmen typischen größeren, fraktal geformten Inseln auch kleinere kreisförmige Inseln. Die Ergebnisse geben zu erkennen, dass diese kleinen, kreisförmigen Strukturen von geordneten Aggregaten in der Adsorptionslösung stammen, und dass sie Ausgangsmaterial für die Bildung größerer Inseln sind. Sie können allerdings nur bei niedrigen Temperaturen beobachtet werden, da sie bei Raumtemperatur wegen der hohen Oberflächenmobilität schnell zu größeren Einheiten zusammenwachsen.

Schließlich wurde das Wechselspiel zwischen Temperatur und Wasserkonzentration untersucht. Dazu wurde die Größenverteilung von Spezies in der Ausgangslösung mit dynamischer Lichtstreuung studiert. Es zeigte sich eine unimodale Größenverteilung von hochgeordneten Aggregaten in Lösung mit einem hydrodynamischen Radius von 200 nm ergab, unabhängig von Temperatur und Wasserkonzentration. Allerdings bildeten sich diese Aggregate bei höheren Wassergehalten und geringen Temperaturen schneller. Weiters wurde auch hier eine charakteristische Temperatur gefunden, die bei größeren Wasserkonzentrationen höher ist, über der derartige Aggregate nicht mehr detektiert werden konnten. Unter dieser Temperatur wurde ein Anstieg der Aggregatkonzentration beobachtet, der etwa 5°C unterhalb der charakteristischen Temperatur in einem Plateau mit konstanter Aggregatkonzentration endet. AFM- und Ellipsometrie-Messungen der korrespondierenden Submonolagenfilme zeigten, dass dieser Temperaturbereich mit einem Übergang von langsamem, homogenem Wachstum zu schnellem Inselwachstum in Zusammenhang steht. Die Resultate wurden hinsichtlich Diffusions- bzw. Adsorptions-limitierung des Abscheideprozesses diskutiert.

Zusammenfassend kann gesagt werden, dass der Wachstumsmechanismus von Octadecylsiloxanmonofilmen stark von der Wasserkonzentration und der Temperatur des Lösungsmittels beeinflusst wird, und dass diese beiden Parameter nicht getrennt von einander betrachtet werden können. Für jede definierte Wasserkonzentration entscheidet die Temperatur, ob diffusions- oder adsorptionslimitiertes Wachstum vorherrscht, und ob hochgeordnetes oder homogenes Wachstum auftritt. Schließlich haben die Ordnungsprozesse in der Lösung vor dem Eintauchen des Wafers einen entscheidenden Einfluss auf die Eigenschaften der erhaltenen Filme.

2 Acknowledgment

I would like to sincerely thank Prof. Gernot Friedbacher for his support and guidance during my thesis in his research group of Micro- & Nanonanalysis. Thanks for seriously introducing me to the methods of surface analysis and for enjoyably adding a personal component to the productive teamwork.

I would also like to thank Prof. Helmuth Hoffmann for the supremely insightful discussions and the perfect cooperation with his workgroup in the Division of Inorganic Chemistry at the Institute of Applied Synthetic Chemistry.

Very special thanks to Hans Foisner who – apart from being a trusted colleague – has become a very near friend. Big thanks also go to Clemens Müllner and Christoph Rill for introducing useful software tools and particularly for their excellent friendship. Furthermore, Christian Sohar shall be thanked for being a reliable colleague, though the duration of our cooperation was very short. I extend my thanks to all students, who have supported this work by their laboratory courses in our group.

Huge thanks go to my friends for accompanying me through my hitherto life and my long lasting study. I am proud of having friends like you.

I want to sincerely express my gratitude to my family; especially my parents and my sister, for their trust and continuing support and all their words of encouragement during my studies. Finally, I want to humbly thank my beloved Sabine, I could not have gotten anywhere near this point without her love and support.

3 Table of Contents

1 Abstract / Kurzfassung 1

1.1 Abstract 1

1.2 Kurzfassung 3

2 Acknowledgment 5

3 Table of Contents 6

4 List of Abbreviations 8

5 Introduction 9

5.1 Self-Assembly and Self-Assembled Monolayers 9

5.2 Octadecylsiloxane (ODS) on Silicon and related SAMs 11

5.2.1 General 11

5.2.2 Deposition Parameters 12

5.3 Motivation of this Work 17

6 Experimental 19

6.1 Atomic Force Microscopy 19

6.2 Ellipsometry 21

6.3 Karl-Fischer Measurements 22

6.4 Dynamic Light Scattering 23

6.5 Sample Preparation 24

6.5.1 Chemicals and Materials 24

6.5.2 Wafer Preparation 24

6.5.3 Preparation of the Adsorption Solution 25

6.5.4 Adsorption Experiments 25

6.5.5 Temperature Control 26

6.5.6 Wafer Post-Treatment 27

6.5.7 AFM Image Processing 27
6.5.8 Quantitative Image Evaluation 29

7 Results and Discussion 30

7.1 Preliminary Experiments 30
7.1.1 Adjustment of the Water Concentration 30
7.1.2 Treatment of the Wafer Substrates after Adsorption 35
7.2 The Influence of the Water Concentration on the Deposition Behavior 39
7.3 The Influence of the Temperature on the Deposition Behavior 44
7.3.1 Experiments at a Water Concentration of 10 mmol/L 46
7.3.2 Experiments at a Water Concentration of 12 mmol/L 49
7.3.3 Experiments at a Water Concentration of 15 mmol/L 53
7.3.4 Experiments at Water Concentrations of 8 and 18 mmol/L 60
7.3.5 Adsorption Experiments at Low Temperatures 61
7.4 The Interplay between the Water Concentration and the Temperature 64

8 Conclusion 72

9 Index of Figures 76

10 Index of Tables 80

11 References 81

4 List of Abbreviations

Table 1: *List of Abbreviations.*

AFM	Atomic Force Microscopy
DLS	Dynamic Light Scattering
FDTS	1H, 1H, 2H, 2H-perFluoroDecylTrichloroSilane
HPLC	High (Pressure) Performance Liquid Chromatography
HREELS	High Resolution Electron Energy Loss Spectroscopy
HTS	*n*-HexadecylTrichloroSilane
NMR	Nuclear Magnetic Resonance
ODS	OctaDecylSiloxane
OMBD	Organic Molecular Beam Deposition
OMBE	Organic Molecular Beam Epitaxy
OPA	OctadecylPhosphonic Acid
OTS	OctadecylTrichloroSilane
SA	Self-Assembly
SAM	Self-Assembled Monolayer
SFG	Sum Frequency Generation
SPM	Scanning Probe Microscopy
STM	Scanning Tunneling Microscopy
TOF-SIMS	Time Of Flight – Secondary Ion Mass Spectrometry
XRR	X-Ray Reflectivity

5 Introduction

In recent years, a complementary approach to inorganic ultra-thin films has come to the fore, organic thin films. The formation of such organic thin films has been increasingly explored, utilizing especially the self-assembly (SA) technique, but also spincoating, organic molecular beam deposition (OMBD), or organic molecular beam epitaxy (OMBE)[1] and Langmuir-Blodgett deposition. The benefit of using organic rather than inorganic material is mainly the innumerable number of molecules that can be synthesized exhibiting an extremely wide variety of functionality. Furthermore, these organic molecules can be designed in such a way that they deposit onto a solid substrate, such as silicon, in a self-limiting manner, so that only one monolayer of the molecules is deposited. This level of control of both the functionality and the morphological parameters of a film is difficult for inorganic techniques, requiring expensive cleanrooms, ultra-high vacuum systems, and ultrapure materials. In contrast, chemists can much more easily create self-assembled monolayers (SAMs) of organic materials in standard, or near standard, environments. Hence, it is not surprising, that different applications for organic thin films were developed. Possible applications can be found in the fields of sensor research[2], biotechnology[2,3,4,5], electronic devices[6], protective coatings in corrosion science[7], tribology[89], and nano-structuring[10].

5.1 Self-Assembly and Self-Assembled Monolayers

Molecular self-assembly is an important phenomenon in nature. For instance, DNA replication and the build-up of living cells and biomembranes satisfy the criteria of self-assembly. Self-assembly is a process in which atoms, molecules, and aggregates of molecules and components arrange themselves in ordered functioning entities without the aid of human manipulation. These assemblies often show new functions and properties that cannot be exhibited by the isolated monomer.

This technique, when applied to the area of thin films, refers to the spontaneous formation of a monolayer of organic molecules on a surface. A

molecule able to build a SAM at least consists of three specific regions: a headgroup which chemically bonds to a solid substrate, the body of the molecule which constitutes the bulk of the film and exhibits essential molecule-molecule interactions (i.e. steric and van der Waals) necessary for stabilization of the ordered films, and the tailgroup which terminates the film surface and determines the surface functionality of the film, such as hydrophobicity, biological sensitivity, and passivation. Typically, these molecules are transferred to the solid substrate by means of a low concentration solution in an organic solvent and immersing a substrate into the solution for a certain period of time. Figure 1 shows a scheme of such a monolayer formation.

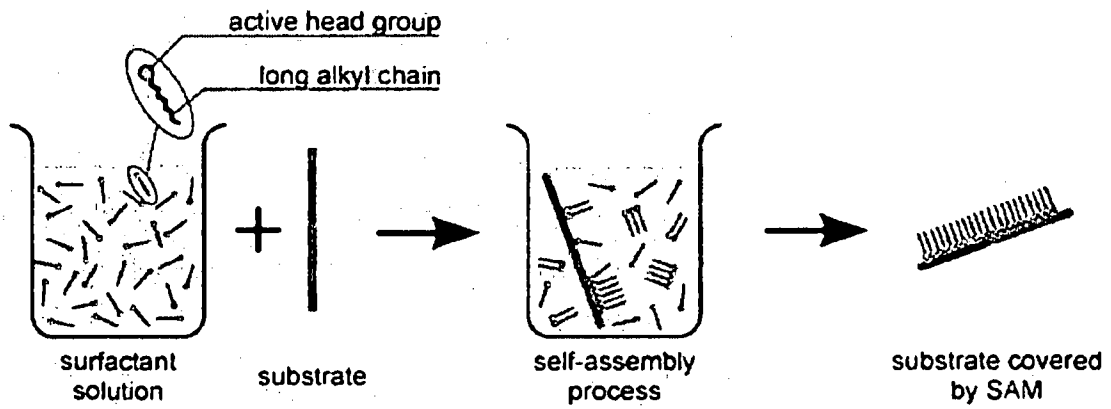

Figure 1: *Scheme of the formation of a self-assembled monolayer (SAM)*[11].

Only a few systems have been found that form complete monolayers through chemisorption onto a solid substrate. The two most common are organosilicon compounds on hydroxylated surfaces and organosulfur compounds on noble metals. Others are fatty acids on metals and metal oxides that have been studied first by Allara and Nuzzo[12], alkylphosphonic acids (e.g. octadecylphosphonic acid, OPA) on metal and non-metal surfaces investigated by Woodward et al.[13], amines on gold[14], or alkenes deposited on hydrogen-terminated silicon substrates by forming direct Si-C bonds[15]. By far the strongest covalent bonds are the Si-O bonds formed between silanes and OH-terminated oxides (130 kcal/mol)[16] followed by the S-Au bonds formed between thiols and gold substrates (40-45 kcal/mol)[17]. The acid molecules bond to the substrate ionically rather than covalently and therefore are less strongly

attached. The strength of these exothermic headgroup-substrate interactions drives the reaction to formation of complete monolayers.

5.2 Octadecylsiloxane (ODS) on Silicon and related SAMs

5.2.1 General

The self-assembly mechanism for this system was first investigated by Maoz and Sagiv[18] and was later described by other groups[19,20,21]. Although, formation of self-assembled monolayers of n-alkyltrichlorosilanes is associated with great problems concerning reproducibility, organosilanes adsorbed on a widespread variety of substrate materials became one of the most popular SAM systems. Due to their desirable properties of high chemical and mechanical robustness, a variety of experimental techniques has been utilized to investigate film formation and properties of resulting monolayer films.

The film thickness of a full monolayer of ODS on silicon was determined using x-ray reflectivity (XRR)[22,23,24,25,26], ellipsometry[24,25,26], and AFM[26,27,28,29,30] revealing thicknesses of 20-29 Å compared to a calculated molecular length of 26.2 Å, which indicate the ODS molecules to be approximately vertically oriented. Komeda et al. found lower thicknesses with AFM which they explained by the action of the AFM tip[31,32]. Moreover, the AFM results showed that complete ODS films are very smooth (rms roughness < 1 to 3 Å). Vallant et al. calculated a tilt angle of 7 ± 1° for a complete film from their IR data[33]. Allara et al. found a best fit for their IR spectra with a molecular tilt angle of 10 ± 2° [50]. Furthermore, IR spectroscopy studies revealed that complete, ordered ODS films have a CH_2 anti-symmetric stretch vibration at 2918 cm^{-1} corresponding to an all-trans conformation. This frequency shifts to higher values if the films are unordered[27,34,52]. The all-trans conformation is also confirmed by water contact angle measurements[23,24,25,26] that showed extremely hydrophobic layers with contact angles between 112° and 114° suggesting the terminal methyl groups to be primarily exposed. Finally, the density of the closely packed monolayer was found to be 0.43 ± 0.05 ρ_{Si} (ρ_{Si} is the density of silicon atoms in the <100>

surface) which was used to calculate an average area per molecule of 20.2 – 22.5 Å² [22,24,25,35]. Moreover, many other techniques like sum frequency generation (SFG)[36], raman spectroscpopy[37,38], HREELS[39,40], TOF-SIMS[4142], or NMR[19,37] have been used to investigate the degree of order of the films.

Apart from the determination of the properties of complete films, also growth studies were performed to shed more light on the growth mechanism. However, neither monolayer growth via islands[43,44] nor uniform layer growth[24] as well as the parameters that lead to a change in the growth mechanism are fully understood yet.

5.2.2 Deposition Parameters

5.2.2.1 Substrate, precursor concentration, solvent, chain length, and solution age

Several deposition parameters are of crucial importance for the production of well defined highly ordered films. A comparison of the deposition behavior of OTS on silicon and mica surfaces has been reported by Brunner et al.[45]. The silanol groups of the silicon substrate act as binding sites restricting surface diffusion of OTS precursor molecules on the surface. In contrast to the silicon surface, mica exhibits a negligible number of hydroxyl groups. Thus, on silicon a higher number of distinctly smaller islands that show a more fractal-like shape are observed. Brunner et al. produced a single silicon oxide monolayer on mica by depositing a complete ODS monolayer and oxidizing the hydrocarbon chains afterwards. Subsequent sub-monolayer deposition of ODS led to a pronounced change in the morphology of the resulting islands. The authors concluded that the island morphology and structure are controlled by the number of reactive sites on the substrate surface. Due to the fact that an increasing number of silicon oxide layers led to a continuous decrease of adsorption rates, the different adsorption rates on mica and silicon were suggested to arise from the negative surface charge of freshly cleaved mica. As this charge of mica may cause attractive forces between the polar head group of the OTS molecule, which enhance adsorption of ODS on mica, a shielding of these forces due to the silicon oxide layer, decreases the adsorption rates. Finally, Terrill et al.[46] found that a decreasing surface roughness of their gold substrates results in a significant increase in adsorption rate and film thickness.

Terrill et al. also investigated the influence of the precursor solution and found that an increase of the thiol concentration from 0.001 to 10 mmol/L leads to an increasing adsorption rate. In general, such a result is of course expected for adsorption experiments, however, for self-assembly adsorption more complex relations between concentration and adsorption rate can occur. For instance, Foisner et al.[47,48] found that high OTS concentrations of up 50 mmol/L lead to adsorption of irregular rough films with lower density and that full monolayer coverage cannot be achieved due to disordered organic molecules passivating the surface.

Rozlosnik et al.[49] emphasized the influence of the solvent on the growth of self-assembled monolayers. They found that deposition from solvents with a medium water solubility like heptane results in highly ordered complete films whereas deposition from solvents with low water solubility like dodecane yields in ODS multilayers. Associated with these findings, it has to be noted that a great variety of different solvents like several n-alkanes[49,50], toluene[44], and even solvent mixtures like bicyclohexyl / THF[51], CCl_4 / isobar G[52], or hexadecane / CCl_4[50] have been used for the investigation of the growth of SAMs. Thus, widely controversial interpretations on the deposition mechanism are found in literature. Moreover, due to a lack of awareness of their importance some reports do not include information on water concentration and mixing ratios of the solvents. Therefore, comparison of results from different authors with each other and the work described in this thesis is often very difficult or even impossible.

The influence of the chain length on the deposition behavior of alkylsiloxanes was investigated by numerous groups[33,39,47,48,53] as well. In general, growth via islands was only found for longer chain lengths, while for molecules with chain lengths < C_6 the resulting layers are less densely packed. Due to blocking of reactive sites and a decreased diffusion rate of the molecules in the solution precursor molecules with longer chain lengths need longer for ordering and deposition. Lower film order for shorter chain lengths was explained by reduced van der Waals interaction energies between adjacent hydrocarbon chains. Utilizing AFM, Lio et al.[54] found that for precursor molecules with chain lengths greater than C_8 - C_{10}, the frictional behavior is very similar, whereas shorter chain lengths showed a strong dependence of the friction from the chainlength, which was again attributed to less densely packed monolayers of the molecules with shorter carbon chains. Finally, the

chain length was found to influence the critical temperature found for the deposition of alkylsiloxane monolayers on silicon[51,60], which will be addressed below.

Finally, a further deposition parameter, which has been investigated, is the solution age. Angst and Simmons[52] showed, that OTS molecules in solution can pre-polymerize, when the solution is allowed to age. Other studies confirmed the influence of the solution maturation and found an optimum maturation time of 10 minutes for a given deposition time[44,55]. Foisner et al.[47] observed that for low OTS concentrations in the solvent a short maturation time of 20 s is sufficient in order to achieve highly ordered monolayers, whereas when working with high concentrations of 50 mmol/L longer maturation times of 10 min are needed.

5.2.2.2 Water and Temperature

Silane chemistry relies on water to hydrolyze chlorosilane groups into silanol groups, which, in turn, are needed for film formation. However, the water was found to be of crucial importance not only for hydrolysis, but also for several effects on the substrate surface. In fact, Britt and Hlady[29] found that on completely dry mica substrates OTS film formation does not occur.

On a native silicon surface, the density of hydroxyl groups is approximately 1 per 20 Å² under atmospheric conditions[24] which corresponds to $5*10^{14}$ hydroxyl groups per cm², which is close to the packing density of ODS molecules (see 5.2.1). However, it seems unlikely that all ODS molecules are able to chemically adsorb to the surface. Complete films rather form through neighbor cross-linking of the precursor molecules. Le Grange et al.[56] compared film formation on dehydrated, partially dehydrated, and hydrated silica substrates. From their results with ellipsometry they estimated that only 1 out of 5 ODS molecules is directly bonded to the surface. Angst and Simmons[52] addressed the degree of cross-linking in the monolayers, as they suggested the molecules in the complete film to contain many siloxane groups bonded to water molecules. Only curing at 150°C forced the siloxane groups to react and form Si-O-Si bonds.

In fact, most authors agree that the surface OH-concentration has a strong influence on the formation and quality of the deposited films. Most interestingly, Allara et al.[50] found with ellipsometry, IR spectroscopy, and contact angle measurements, that ODS films on silicon oxide and on hydrated gold substrates

without surface hydroxyl groups show the same properties, indicating that the films exhibit the same, high conformational order. The authors conclude, that few bonds form between the ODS molecules and the substrate and that the water film on the substrate is most probably responsible for film formation. This finding was also affirmed by Zhao et al.[64] using second harmonic generation. Finally, the fact that a mica surface, being a frequently investigated substrate for ODS deposition[e.g.11,20], is also able to exhibit full monolayer coverage, although it is almost entirely deficient of hydroxyl groups[57], supports this conclusion. It has to be noted, however, that the growth behavior on mica is significantly different from growth on silicon.

In contrast to that Rye et al.[58] found with XPS and SIMS that the coverage of OTS on vacuum-fired substrates was approximately only 1/3 of the coverage achieved on hydrated substrates under otherwise identical conditions. This indicates that surface OH groups, able to form chemical bonds with the film molecules, are required to achieve full coverage. With SIMS Rye found strong peaks for SiOH fragments on uncovered substrates that disappear almost completely for complete films, indicating that the surface silanol groups are consumed in the SAM formation process. Although Rye proposes that nucleation of the film only occurs at surface OH groups this author states that the water layer is also important for complete film formation. Moreover with octadecyldimethylchlorosilane (ODMS) a coverage of approximately 30% – compared to OTS – could be achieved on hydrated substrates. This indicates that substantial film growth through formation of siloxane bonds between surface OH-groups and film molecules can also be achieved without cross-linking between the precursor molecules which is blocked for ODMS.

The strong influence of the water concentration in the adsorption solution has been reported by Leitner et al.[44]. In their studies toluene has been used as solvent. The authors found strongly increasing growth rates as well as increasing sizes of sub-monolayer islands on silicon with increasing water concentrations in the range from 5 to 13 mmol/L. Bunker et al. have investigated the influence of the water content for a different system - 1H, 1H, 2H, 2H-perfluorodecyltrichlorosilane (FDTS) in isooctane[59]. The films have been characterized with atomic force microscopy (AFM) and contact angle measurements. The adsorption solution has been investigated with ^{17}O-NMR and dynamic light scattering (DLS). The authors found that hydrolysis of the silane precursor in the solution is comparatively fast, and thus not the limiting factor for film growth. Furthermore, DLS measurements revealed the

formation of larger species in the solution with hydrodynamic radii of up to 800 nm depending on the water concentration. Within the first minutes of the experiments scattering intensities were observed to be very low. Then, a burst of the signal was detected due to formation of aggregates which continued to grow until a maximum size was reached. Although the authors were not sure about the exact nature of these aggregates they reported that these features may be inverse micelles, micelle aggregates, inverse vesicles, or nested vesicles. They concluded that these aggregates adsorb onto the substrate surface which was supported by observation of corresponding features in the AFM images. The suggestion that the appearance of fractally shaped islands indicates that clusters of molecules formed in solution attach to the surface was previously made by Bierbaum et al.[53].

One of the first parameters which has been described, the deposition temperature, was found to show a huge impact on the growth of organosiloxane monolayers and seemed to be crucial for obtaining reproducible results from deposition experiments. Brzoska et al.[60] investigated the critical surface tensions for alkylsiloxanes as a function of the temperature in dependency on the number of methylene units, n. They found, that a critical temperature, T_c, exists, above which the surface tension increases indicating a more disorganized film. This critical temperature increases linearly with the chain length by 3.5 ± 0.5°C for each additional methylene group which was confirmed by Ilmura et al.[51]. For n = 18, octadecylsiloxane, T_c ~ 28°C was found. Parikh et al.[61] confirmed these findings and found T_C = 28 ± 5°C for octadecyltrichlorosilane deposition. Below this temperature highly ordered films or densely packed islands have been obtained. Above this critical temperature only disordered films have been observed. With increasing temperature the measured coverage decreases. This was explained by Rye[62] as a consequence of the thermal budget of the silane chains. At elevated temperatures low energy rotations of the C-C bonds can occur, leading to a larger space requirement of the alkane chains compared to a proposed all-trans conformation of the chains in ordered films. In both studies[61,62] the critical temperature T_C has been associated with the triple point of a Langmuir-Blodgett (LB) phase diagram.

Carraro et al.[63] have found three different growth regimes depending on the temperature. Below 16°C island growth has been observed, while above 40°C homogenous disordered growth was found. In the intermediate temperature range they speak of a mixed regime, i.e. a coexistence of a liquid expanded and a liquid

condensed phase similar to the formation mechanism described for LB films. The discrepancies between results from different authors show the complexity of this matter.

The presence of a critical temperature and the fact that most experiments observe little bonding between the adsorbed film and the substrate let film formation appear to occur in the following manner[51,61,64,65]: Firstly, a thin, one to three layers, tenaciously bound water film forms on the surface via hydrogen bonding with the surface OH-groups[52]. This amount of water seems to be formed immediately upon exposure to air, though a dry substrate can still absorb water from an adequately hydrated solution[66]. Then, the silane molecules become physisorbed and hydroxylated in whatsoever order. The hydroxylation takes place either through reaction with trace water in the solution or via the surface bound water. Subsequently, the silanol molecules bond to the water layer via hydrogen bonds. The relatively weak interactions between the adsorbed molecules and the water allow the molecules to diffuse on the surface. At some point, chemical reactions between neighboring precursor molecules take place, linking them together. Finally, condensation reactions lead to bonding of a few of the silanol groups to the substrate.

One of the rare studies dealing with the mutual influence of both parameters, water and temperature, was published by Chen et al.[67]. They found that the critical temperature in the formation of self-assembled *n*-hexadecyltrichlorosilane (HTS) monolayers on mica depends on the water content in the solvent which was dodecane in their work. With a water concentration of 1.5 mmol/L, they found a critical temperature of 31 ± 1°C. When the water content was lowered down to 0.54 mmol/L, no critical temperature was found in the temperature range of 10–55°C. Chen et al. suggested that the critical temperature is lower for increased water contents and that the existence of a critical temperature is due to the deposition of clusters on the mica surface formed in the solution.

5.3 Motivation of this Work

As mentioned above, many interpretations found in literature are somewhat contradictory with respect to the growth mode (island growth and uniform growth are

discussed), adsorption- and diffusion controlled growth, or the role of the water or the deposition temperature. A good deal of these seemingly contradicting results is most probably due to the widely differing systems that have been investigated.

Furthermore, although numerous publications on various growth parameters can be found in literature, hardly anything has been reported on the mutual influence and mutual effects of these parameters. Therefore, this thesis deals with the role of the water concentration of the solvent and the deposition temperature in the growth of octadecylsiloxane films on silicon using toluene as adsorption solvent. Finally, the influence of the interplay of these two parameters on the growth mechanisms should be investigated for the growth of octadecylsiloxane films on silicon in the sub-monolayer regime using atomic force microscopy and ellipsometry. In order to obtain information on the formation of aggregates in the deposition solution dynamic light scattering was performed.

When first experiments were performed in order to study the influence of the water concentration great problems with the reproducibility were recognized. Thus, in the first instance a method had to be found to reproducibly adjust the water concentration of the toluene. For the purpose of investigating the influence of the solution and the deposition temperature, a temperature control unit, suited for mounting in a glove box, was needed combining both chemical inertness (different solvent vapors and gaseous HCl are apparent in the glove box) and high accuracy.

6 Experimental

6.1 Atomic Force Microscopy

In general, atomic force microscopy (AFM) along with a great number of other techniques belongs to the field of scanning probe microscopy (SPM). The first of these techniques which was developed by Binnig and Rohrer[68] in 1982 was the scanning tunnelling microscopy (STM). The first atomic force microscope was built by Binnig, Quate, and Gerber[69] in 1986 in order to overcome the limitation of STM to conductive samples.

All different scanning probe microscopes have in common that by utilization of piezoelectric elements, a very fine tip (with a tip radius typically below 40 nm) is scanned over the sample's surface in very close proximity to or in contact with the sample. The great advantage of these techniques is the avoidance of the Abbe limit for the lateral resolution through scanning in the "near-field", and thus, allowing the achievement of extremely high lateral resolution down to the atomic level. The difference between separate types of microscopes is that in order to obtain the desired sample information, different analytical signals, which are governed by the interaction between the probe and the sample, are used.

In our AFM, a laser beam is focused onto a cantilever and the reflected beam is directed towards a partitioned photodiode via a moveable mirror. As the sample is scanned underneath the tip, the cantilever is deflected resulting in a vertical change of the laser beam position on the photodiode, which can be converted into topographical information.

The AFM images were recorded in tapping mode, which is a key advance in AFM. Tapping mode overcomes problems associated with friction, adhesion, or electrostatic forces by drastically reducing the period of the interaction of the cantilever with the surface. Tapping mode imaging is implemented in ambient air by oscillating the cantilever assembly at or near the cantilever's resonant frequency using a piezoelectric crystal. The piezo motion causes the cantilever to oscillate with an amplitude of typically more than 20 nm when the tip is not in contact with the

surface. The oscillating tip is then moved toward the surface until it begins to slightly touch or tap the surface. The reduction in oscillation amplitude is used to identify and measure surface features. During tapping mode operation in constant amplitude mode, the cantilever oscillation amplitude is maintained constant by a feedback loop controlling the vertical position of the sample. Selection of the optimal oscillation frequency is software-assisted and the force on the sample is set and maintained at the lowest possible level. The oscillation amplitude of the tip is measured by the photo detector and processed by the NanoScope III controller electronics. The digital feedback loop then adjusts the tip-sample separation to maintain constant amplitude and force on the sample.

An alternative of obtaining image contrast with the tapping mode AFM is phase imaging. Phase detection refers to the monitoring of the phase lag between the signal that drives the cantilever to oscillate and the cantilever oscillation output signal. Changes in the phase lag reflect changes in the mechanical and chemical properties of the sample surface like elasticity and adhesion leading to changes in the tip-sample interaction through variation of long- and short-range forces.

A scheme of a tapping mode atomic force microscope as used in this thesis is shown in Figure 2, depicting the components described above.

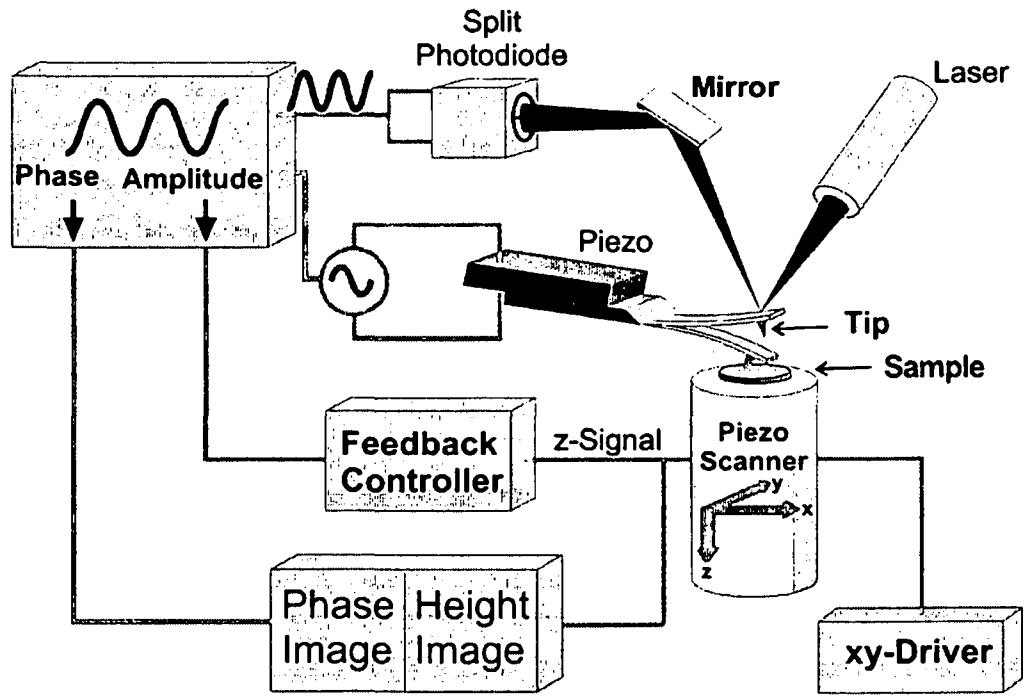

Figure 2: *Scheme of tapping mode atomic force microscopy*[70].

For the work at hand, AFM measurements were accomplished with a Nanoscope III Multimode SPM from Digital Instruments, Veeco Metrology Group, Santa Barbara, CA, under ambient conditions. Pointprobe n^+-silicon cantilevers with integrated silicon tips (Nanosensors, Germany) for tapping mode application with a spring constant of 28 - 52 N/m, a resonance frequency of 290 – 340 kHz, and a resistivity of 0.01 – 0.02 Ωcm were used. Two different piezo scanners were used. AFM images of up to 5 x 5 μm^2 were recorded utilizing an E-scanner with a maximum scan range of 10 x 10 μm^2, larger images of up to 25 x 25 μm^2 were obtained with a J-scanner (100 x 100 μm^2 maximum scan range). The images were recorded in constant amplitude mode with a resolution of 512 x 512 pixels at scanning rates from 1.0 or 2.0 Hz. Data analysis was performed with the NanoScope III software and a custom-programmed software routine described later in 6.5.7 and 6.5.8.

6.2 Ellipsometry

The ellipsometric measurements were performed with a PLASMOS SD 2300 instrument with a rotating analyzer. A He-Ne laser (632.8 nm) was utilized at 68° incidence. A scheme of a rotating angle ellipsometer is shown in Figure 3. Ellipsometry measures the change in polarization state of light reflected from the surface of a sample. A linearly polarized incident beam interacts with the different layers of the sample with its different optical constants and is therefore converted to an elliptically polarized reflected beam. For any angle of incidence greater than 0° and less than 90°, p-polarized and s-polarized light will be reflected differently. The measured values are expressed as the amplitude ratio Ψ and the relative phase shift Δ. These values are related to the ratio of the Fresnel reflection coefficients, R_p and R_s for *p* and *s*-polarized light, respectively.

$$\tan(\Psi)e^{i\Delta} = \frac{R_p}{R_s}$$

Since ellipsometry measures the ratio of two values rather than the absolute values of either, it can be highly accurate and very reproducible. For instance, it is insensitive to scatter and fluctuations, and in principal requires no standard or calibration.

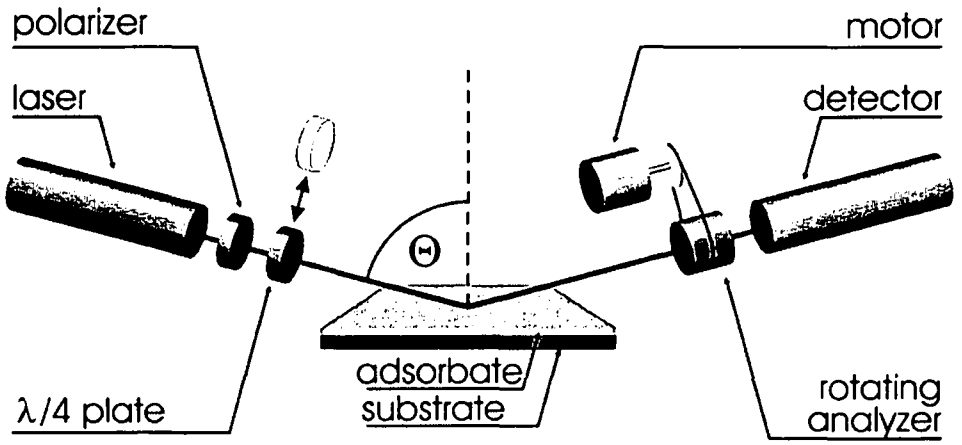

Figure 3: *Scheme of rotating angle ellipsometer*[71].

Determination of the silicon oxide film thickness and the organic film thickness is based on a model of three layers (Si / SiO_X / air) and a four-phase model (Si / SiO_X / adsorbate / air), respectively. The usage of the four-phase model requires the thickness of the silicon oxide film thickness to be known. A commercial software based on the McCrackin algorithm[72] was used to calculate the film thickness from the measured ellipsometric angles (relative phase shift Δ and amplitude ratio Ψ) by means of given refractive indices and adsorption coefficients for all layers. Literature values were used for all optical constants of the layers[73]. For each sample 5 different spots were measured and the average value was determined. In this manner typical standard deviations between 0.01 and 0.05 nm have been obtained.

6.3 Karl-Fischer Measurements

The determination of the water content of toluene was carried out utilizing a commercial Karl-Fischer-setup, a Metrohm Karl-Fischer Automat E547 using Hydranal Composite 1 (Riedel-de-Haën) as reagent. The volumetric titration is based on the reaction

$$I_2 + SO_2 + 2H_2O \rightarrow 2HI + H_2SO_4$$

in the presence of typically imidazole as a base and methanol as a hygroscopic solvent. The titration endpoint is determined coulometrically.

First, the titer of the Karl-Fischer-reagent was determined by titration of bidistilled, deionized water. Approximately 2 µL water were dripped into a small

platinum pot using a 2-µL Hamilton Microliter Syringe and the exact amount of water was determined by weighing with an analytical balance. Then the platinum pot was put into the methanol solution of the Karl-Fischer-titrator and automatic titration was performed until equilibrium was reached. The titer of the Karl-Fischer reagent was obtained by averaging the results of 4 individual titrations.

For the determination of the water content in the adsorption solutions, 3 mL toluene were pipetted directly into the reaction vessel using an Eppendorf pipette and automatic titration was again performed until equilibrium was reached. The water content of the toluene was obtained by averaging the results of 3 individual titrations.

6.4 Dynamic Light Scattering

For the thesis at hand, dynamic light scattering (DLS) experiments were performed in order to investigate the influence of processes in the deposition solution on the growth process. Here, only a short introduction into the principles of DLS is given, for further details refer to refs. 74, 75, 76.

In short, through utilization of laser pulses it is possible to monitor the Brownian molecular motions of the particles or molecules in solution. Due to the Doppler effect, these motions lead to frequency shifts in the scattered radiation. These very small shifts in frequency result in a broadening of the spectral lines which is proportional to the diffusion coefficient of the particles or molecules. However, not the so-called Doppler shift spectrum is recorded but the fluctuations of the scattering intensity are determined by autocorrelation of the time-resolved scattering intensities. Thus, it is possible to calculate the translational diffusion coefficient. From this coefficient the hydrodynamic radius can be computed using the Stokes-Einstein equation

$$D = \frac{k_B T}{6\pi\eta R_h}$$

wherein k_B is the Boltzmann constant, T is the absolute temperature, η is the dynamic viscosity and R_h is the hydrodynamic radius of the particle or macromolecule.

Size distribution measurements in solution were carried out using an ALV CGS-3 compact goniometer system with a He-Ne laser (wavelength λ = 632.8 nm). The

detector angle was fixed at 90°. The temperature was exactly controlled via a peltier element. The detection system consists of a photomultiplier and an autocorrelator to calculate the correlation function by recording the intensity versus time. Operation and analysis was performed utilizing commercial software (ALV-Correlator software V.3.0).

6.5 Sample Preparation

6.5.1 Chemicals and Materials

A list of chemicals utilized for the preparation of samples is depicted in Table 2.

Table 2: *List of chemicals used for this work.*

Chemical	Specification	Manufacturer
octadecyltrichlorosilane (OTS)	> 96%	Merck GmbH
toluene, HPLC-grade	99.8%	Sigma-Aldrich Handels GmbH
acetone	99.9+%	Sigma-Aldrich Handels GmbH
ethanol	99.8%	Hefe Austria AG
nitrogen gas	99.999%	Air Liquide GmbH
Hydranal Composite 1		Riedel-de-Haën

For all experiments silicon wafers from Wacker Siltronics AG were used. The wafers were prime grade, single side polished CZ-Si discs with a diameter of 100 mm and a thickness of 500 – 550 µm. P-type (boron) wafers with a crystallographic orientation of <100> and a resistivity 7 – 21 Ohm/cm were utilized.

6.5.2 Wafer Preparation

The wafers were cut into pieces of 1x1 cm^2 in size. Subsequently, the wafers were rinsed with toluene and cleaned with a toluene-soaked tissue. Then they were treated in toluene in an ultrasonic bath for 5 minutes, followed by rinsing with toluene, acetone, and ethanol. Then, the wafers were dried as fast as possible in a nitrogen stream to prevent solvents to leave back traces of impurities on the wafer.

Afterwards, the pieces were put in a UV-chamber (UV-CLEAN, Boekel, Germany) for 15 minutes to remove organic impurities and to activate the surface for the adsorption process by formation of silicon oxide and silanol groups. The resulting oxide layer thicknesses were determined by ellipsometry. Immediately after the measurements, the pieces were stored in Petri dishes and transferred into the glove box with nitrogen atmosphere, where the deposition experiments took place.

6.5.3 Preparation of the Adsorption Solution

Monolayers of alkylsiloxanes were prepared from solutions of 1 mmol/L octadecyltrichlorosilane in toluene. Firstly, the water concentration of the HPLC-grade toluene was determined. Then the desired water concentration was adjusted by doping with a calculated amount of bidistilled, de-ionized water using an Eppendorf research pipette. To keep interactions between the solvent and the surrounding atmosphere to a minimum the solutions were prepared in lever-lid glasses. The solutions were magnetically stirred over night. Finally, the resulting water concentration of the solvent was determined by Karl Fischer titration. For further experiments, the solvent was only used, if the determined water concentration was in good agreement with the nominal concentration based on the amount of doped water. During the whole procedure, both solvent preparation and adsorption experiments, handling with open lever-lid glasses was kept as short as possible, in order to avoid interaction with the surrounding atmosphere. In this way an accuracy of approximately ± 0.5 mmol/L (~ 3%) could be achieved.

6.5.4 Adsorption Experiments

All experiments were performed under nitrogen atmosphere in a glove box. Unless noted otherwise the deposition experiments were carried out in the following manner: Toluene with the adjusted water content was pipetted into lever-lid glass jars. The lever-lid glasses were placed in a temperature control unit (see 6.5.5) and left for temperature equalization for approximately 5 minutes[48]. Then, the OTS concentration was adjusted using an Eppendorf pipette. Thereafter the solution was allowed maturing for 10 minutes. Afterwards, the wafers were immersed vertically in

the solutions for a distinct period of time. Immersion and extraction of the wafers was performed as reproducible as possible with respect to time of the motion, inclination of the substrate and immersion depth. Finally, the reaction was quenched by submerging the samples in HPLC-grade toluene followed by storage in toluene.

6.5.5 Temperature Control

In order to improve the reproducibility of the experiments and to be able to study temperature effects on self-assembly growth, a temperature control unit was developed. For this purpose an aluminum block with 10 recesses for deposition vessels was manufactured (Figure 4). The temperature is measured by a sensor in the metal block and a control unit compares the observed values with the set values. A thermal insulation shell assures minimal thermal losses. Cooling and heating is performed by a thermoelectric peltier device. The heat produced by peltier-cooling of the metal block is discharged by a cooling water circuit, which was crafted especially for the requirement of maximum aridness in the glove box.

The cooling and heating rates at the different recesses were investigated by J. Foisner[48]. He found that the nominal temperature ± 1°C is reached within 5 minutes for all positions. Therefore vessels put into the temperature control unit were left for temperature adjustment for at least 5 minutes.

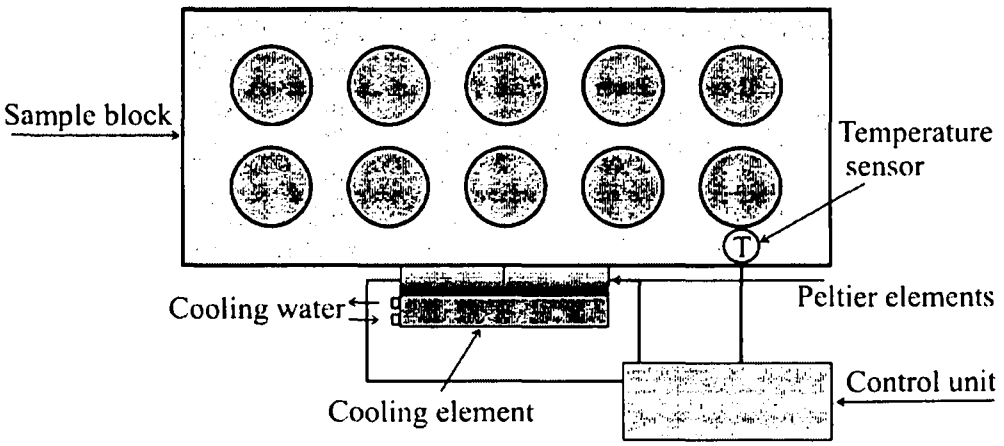

Figure 4: *Schematic diagram of a home-built temperature control unit (thermal insulation shell not shown). Dimensions of the sample block: h/w/d = 5/17/7 cm (with thermal insulation shell: h/w/d = 6/19/11.5 cm).*

In this way, temperature effects in the range between 2 and 35°C and with a temperature resolution of well below 1°C could be studied under otherwise constant conditions.

6.5.6 Wafer Post-Treatment

After the transfer out of the glove box, the wafers were cleaned in toluene and ethanol in an ultrasonic bath for 5 minutes in each case. Subsequently, they were rinsed with toluene, acetone, and ethanol, and dried in a nitrogen stream. After wiping with a tissue, which was previously drenched in HPLC-grade toluene this cleaning procedure was repeated once. Finally, the sample was dried a second time in a nitrogen jet.

6.5.7 AFM Image Processing

Due to scanner hysteresis, especially for large image areas, the raw data routinely obtained by AFM measurements are hardly ever directly suited for quantitative evaluation. Additionally, the absolute height signal delivered by the AFM frequently increases or decreases in jumps from one scan line to the next, thereby introducing horizontal steps into the image which have nothing to do with the actual sample topography. These effects must be eliminated by applying software algorithms to the image data prior to image evaluation. The most important step during image processing is the flattening of the images by fitting the surface usually with a polynomial function line by line and subtraction of this function from the raw data[82]. Image processing was performed using a software package custom-developed by C. Müllner[82].

Figure 5 demonstrates the basic steps of the flattening procedure of the mentioned software package. A typical raw data image is depicted in Figure 5a.

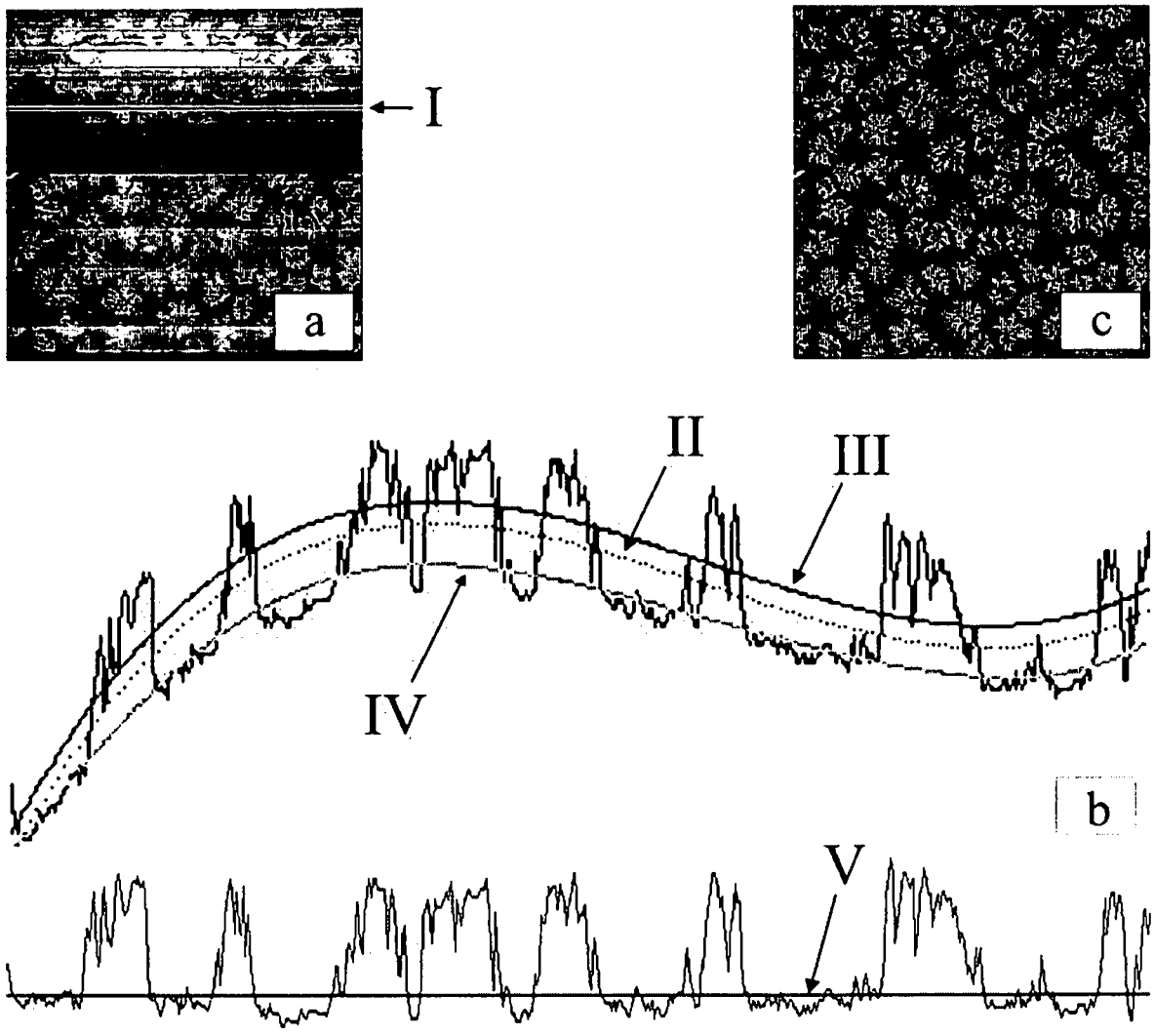

Figure 5: *Image processing as performed with the software package custom-developed by C. Müllner[82]:* ***(a)*** *raw data;* ***(b)*** *line flat of the line in (a) marked with (I);* ***(c)*** *resulting flattened image.*

In short, this routine consists of three basic steps. First, the substrate surface is flattened by subtraction of a multistep polynomial fit of the image height values. Line (II) in Figure 5b represents a 3rd-order polynomial fit of all raw data points along the recorded line. In order to make sure that all data points which belong to the uncovered substrate are below the fitted curve, a constant value is added to all points of the fitted curve (II) resulting in curve(III). Then, a second polynomial fit is performed implementing only those raw data points which are located below curve (III). It can be seen that this second fit (curve (IV)) is a much better approximation of the data points belonging to the uncovered substrate surface. In the final step curve (IV) is subtracted from the raw data leading to a nicely flatted scan line (curve (V)).

This procedure is repeated with all image lines leading to Figure 5c. In addition to this basic concept further algorithms for the treatment of images with special features (e.g. large features or impurity particles) have been used and are described elsewhere[82].

6.5.8 Quantitative Image Evaluation

Image evaluation was performed using the software package custom-developed by C. Müllner[82]. For the determination of the surface coverage of the AFM images, the software computes sum curves from all height values of the image (height values versus number of data points). Through multiple differentiation of this sum curve the number of pixels representing covered and uncovered surface can be distinguished and therefore the calculation of the surface coverage is possible. An example for the distinction of base area (black) and covered area (white) of the wafer depicted in Figure 5 is given in Figure 6a. For evaluation of individual islands, the contiguity of the film is determined by computing next neighbor relationships between the individual data points. Moreover, algorithms were implemented in the software to exclude islands cut due to image boundaries and islands below distinct island sizes. Analysis of the AFM image depicted in Figure 5c performed in this manner reveals islands shown in Figure 6b.

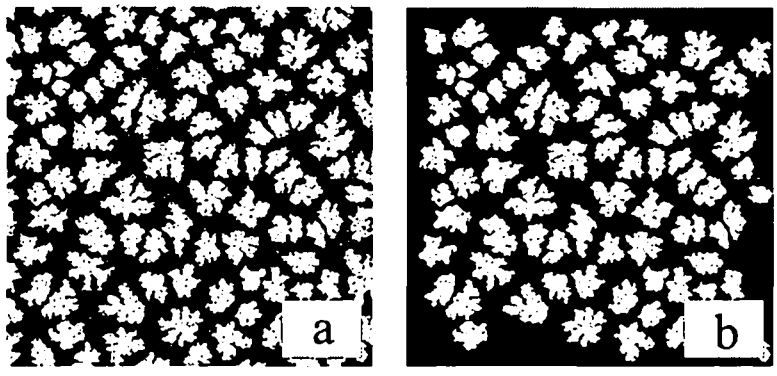

Figure 6: *AFM-images illustrating coverage and island size determination: The images have been obtained by processing the image shown in Figure 5c,* ***(a)*** *determination of the coverage, and* ***(b)*** *determination of the island size distribution.*

7 Results and Discussion

7.1 Preliminary Experiments

7.1.1 Adjustment of the Water Concentration

Various studies on deposition mechanisms of alkylsiloxane monolayer films on silicon have shown an extraordinary role of the concentration of water in the deposition solvent. As the water concentration influences not only the reaction kinetics but is also decisive for the organization of the molecules in solution and therefore the packing density of the resulting monolayer films, the necessity of an exact adjustment of the water content is obvious.

First attempts of controlling the water content in toluene for our adsorption experiments were based on mixing of commercial HPLC grade toluene with low water concentrations with water-saturated toluene. Water saturated toluene was prepared by mixing commercial toluene with an excess of water in a beaker loosly covered with a watchglass. The obtained two-phase system was left to settle in a closed glass bottle for at least 72 hours under normal laboratory conditions, and water-saturated toluene (upper phase) was withdrawn with a pipette for mixing with dry toluene. First adsorption experiments following this procedure exhibited a very bad reproducibility with a scattering of the surface coverages of more than 50%. Cross-check of the water concentration in the adsorption solutions by Karl-Fischer titration showed that large scattering of the water content and significant deviations from the nominal values based on the mixing ratio were the reason for bad reproducibility of the adsorption experiments. Therefore, the procedure for adjusting the water content of our solvent was investigated in more detail.

Freshly opend 2-L bottles of HPLC grade toluene showed water concentrations of 4 to 4.5 mmol/L. Upon repeated opening of a bottle the water concentration of the toluene increased up to 6.5 mmol/L within a period of several days. From that it can be concluded that a changing water content of HPLC grade toluene does not explain the bad reproducibility of experiments performed within the same day or at least on consecutive days. For the water-saturated toluene water

concentrations between 19 and 26 mmol/L have been determined. This comparatively large range, which has sometimes been observed even within one day, can be explained by the varying solubility limit of water in toluene with the temperature. Table 3 shows the solubility of water in toluene for different temperatures taken from different references.

Table 3: *Solubility of H_2O in toluene at various temperatures.*

T [°C]	Solubility [mmol/L]	Ref.
15	20.0 ± 0.06	77
	18.9	78
	13.1	79
25	26.1 ± 0.04	77
	27.4 ± 0.05	80
	25.0	78
	21.0	79
30	29.3 ± 0.04	77
	28.5	78
	25.0	79

Although there are larger differences between values from different sources, the data support that indeed our observed variations of the water concentration can be explained by the temperature-dependent solubility limit of water in toluene. Furthermore, it has been found that toluene with increased water content quickly looses water once separated from the liquid water phase. In order to further clarify the interaction of the humid solvent with the surrounding atmosphere, a simple experiment was performed. A 50-mL beaker filled with 40 mL HPLC-grade toluene was placed in a 100-mL beaker filled with approximately 10 mL of distilled water and the system was closed with parafilm. Then it was left to equilibrate at a temperature of approximately 25°C. After three days the water concentration of the toluene was found to be 24.0 ± 0.5 mmol/L, which is close to the solubility limit of water in toluene at 25°C referring to most of the values given in Table 3.

Concluding, both the temperature-dependent solubility of water in toluene and the humidity-dependent loss of water during sample handling, particularly inside the glove box where the dry atmosphere promotes loss of water, but also outside the

glove box (mixing, Karl-Fischer determination, solvent handling) are the major factors influencing the reproducibility of the adsorption experiments. At this point it should be stressed that working in a glove box is absolutely necessary due to the high moisture sensitivity of OTS.

Since stocking of humidified toluene and mixing as described above is not suited for reproducible experiments, an alternative to this procedure has been pursued. In this alternative procedure the water content of commercial HPLC grade toluene was determined by Karl-Fischer titration, and then a calculated amount of bidistilled water has been directly added using an Eppendorf research pipette. This mixture was prepared in 10-mL lever-lid glasses which were closed after doping the toluene with water. Then, the water was allowed to dissolve by magnetic stirring over night. In order to investigate the feasibility of this procedure, the obtained water concentrations have been cross-checked by Karl-Fischer titration and compared with the nominal values based on the residual water content of the HPLC grade toluene and the amount of water doped. Figure 7 shows the results for 11 water concentrations between 9 and 12 mmol/L. Water determination has been performed both 24 (black squares) and 48 hours (open triangles) after doping. Each data point is the mean value of 3 Karl-Fischer determinations. The whole experiment was repeated four times resulting in eight data points for each water concentration in the diagram.

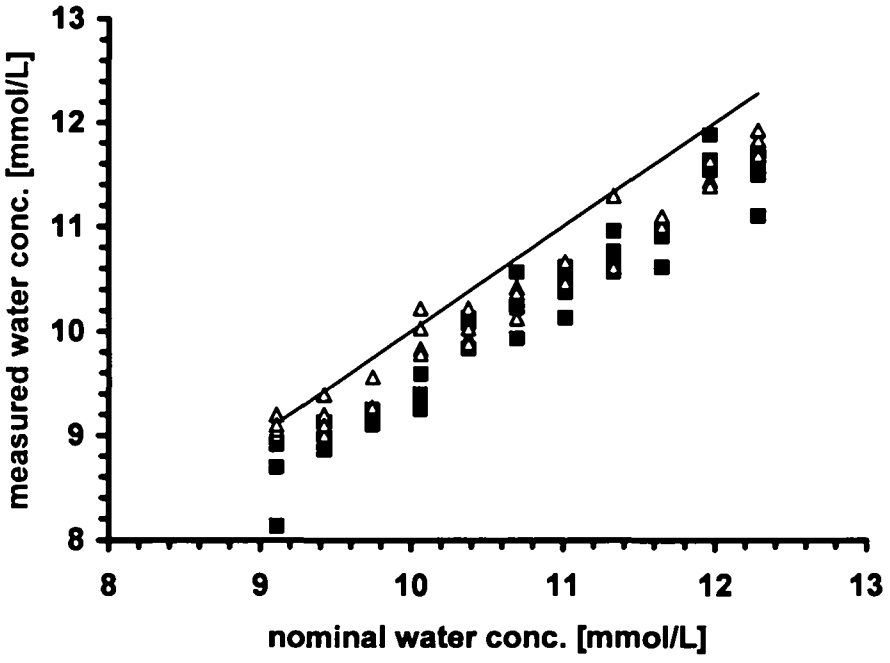

Figure 7: *Water concentrations in toluene determined by Karl-Fischer-titration versus nominal water concentration: titrations have been performed (■) 24 and (Δ) 48 hours after doping with bidistilled water. The data points are mean values from three titrations. The solid line is the median in the diagram. For details refer to the text.*

Across the whole range of water concentrations it can be seen that the determined values are lower then the nominal values (solid line in Figure 7). In order to explain this deviation 3 hypotheses have been considered: matrix effects in the Karl-Fischer determination, incomplete dissolution of the doped water, and loss of water during the procedure. In principle matrix effects (e.g. different side reactions or electrode passivation) in Karl-Fischer determinations are possible[81]. However, such matrix effects are not reported for toluene. In fact, such effects would be very unlikely for this inert solvent of high purity.

Figure 8 shows the relative deviations of the measured water concentrations from the nominal values. The data reflect the mean values of the data points shown in Figure 7. Despite the scatter in the diagram, it can be seen that the deviation for determinations after 48 hours (open triangles) is generally lower than for determinations after 24 hours (black squares). This slight increase of the water concentration shows that loss of water due to evaporation could be successfully avoided by use of the lever-lid glasses.

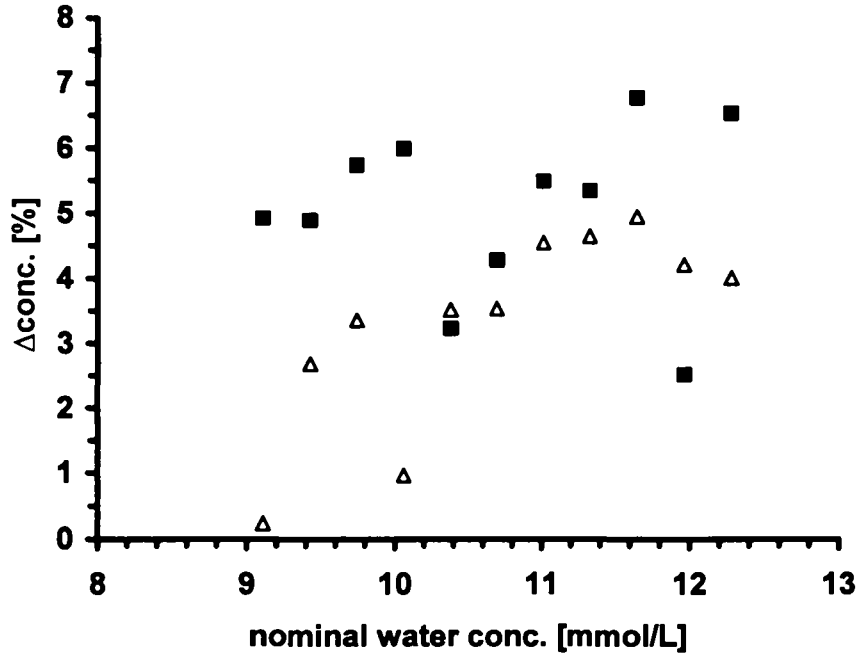

Figure 8: *Relative deviations between measured water concentration in toluene and nominal value: The data points are mean values from four independent experiments. Measurements have been performed (■) 24 and (Δ) 48 hours after doping. For details refer to the text.*

This decreasing deviation from the nominal water concentration also indicates that dissolution of the water in toluene is very slow and not yet complete even after one or two days. This finding may be somewhat surprising, because concentrations well below the solubility limit of water are considered in these experiments. Presumably the dissolution rate strongly decreases with decreasing amount of residual undissolved water in the lever-lid glass. This may be associated with the fact that it is difficult to dissolve the final residue of undissolved water adsorbed or adhering to the glass surface. Finally it should be mentioned that Figure 8 shows a trend of lower deviations between nominal and measured values for lower water concentrations. This indicates that the dissolution kinetics is faster for larger differences between solubility limit and actual concentration, as expected. Moreover, the increasing deviation with increasing water concentration of the solvent could also be explained by increasing evaporation of water during solvent handling due to increasing water vapour pressures. Such an explanation is also supported by larger data scattering at higher water concentrations of 18 mmol/L and more, given the fact that for higher

concentrations reproducibility of sample handling (e.g. contact times with the atmosphere) is particularly critical.

Concluding, the major factor responsible for the negative deviation of the obtained water concentrations from the nominal values is the low dissolution rate of water in toluene under the given conditions. However, waiting for complete equilibration longer than one day is not feasible for practical purposes. Therefore, an other approach has been chosen for all following experiments. In this approach the solvent is doped with an extra amount of water just sufficient to reach the desired water concentration after one day of dissolution. The solvent prepared in this manner must be transferred to a different vessel prior to the adsorption experiments in order to avoid any disturbances from the excess of water, presumably adhering to the glass wall of the preparation vessel. This was found to be the best choice for both accurate and reproducible adjustment of the water content, allowing to control the water concentration with an accuracy of ±3 %.

7.1.2 Treatment of the Wafer Substrates after Adsorption

When first deposition experiments were performed in this thesis a relatively easy and timesaving cleaning procedure for the wafers after the deposition was introduced.

The wafers were rinsed and stored in toluene in the glove box subsequent to the deposition experiment. After the discharge from the glove box the wafers were wiped with a tissue drenched in toluene, treated in toluene in an ultrasonic bath for 5 minutes, thereafter rinsed with toluene, acetone, and ethanol, and finally dried in a nitrogen stream.

Wafers treated in this manner typically showed scratches heading mostly parallel through the AFM images. An example for such an image can be seen in Figure 9a. The scratches are differing in depth and due to the fact that they can only be observed on ODS-covered surfaces (within islands or full monolayers), the number of visible scratches increases with increasing surface coverage. Using the AFM images for simple visualization purposes, these scratches are not critical.

However, major problems occur when such images are processed with algorithms for the determination of the island sizes and the surface coverages. As the

scratches cut through the islands, island size determinations are only possible with highly sophisticated algorithms to deduct the scratches. At higher coverages even these algorithms fail.

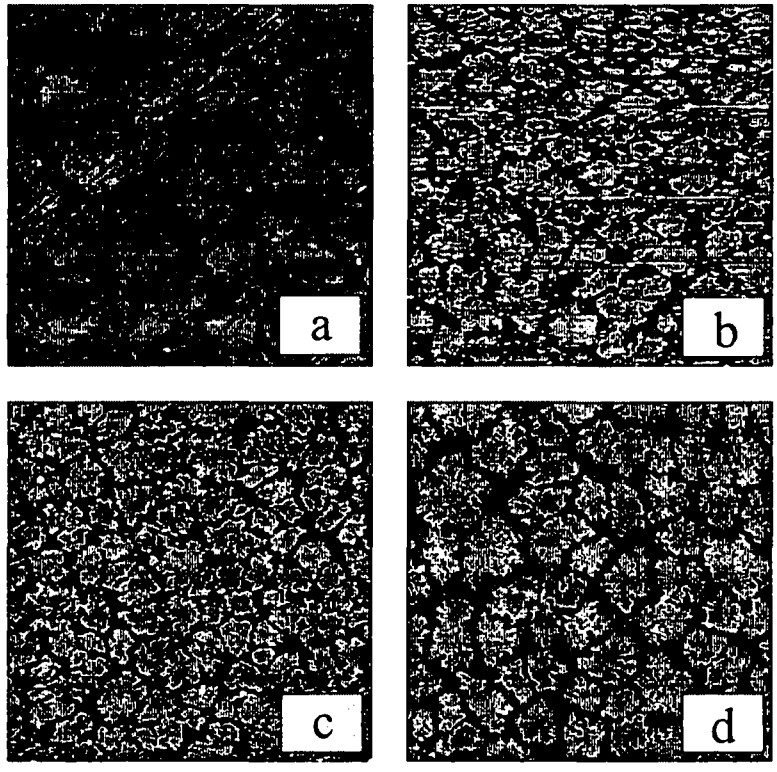

Figure 9: *AFM images of ODS on silicon illustrating the different possibilities of treatment of the wafer pieces after the deposition experiment: for sake of lucidity the treatment steps are given in Table 4.*

The treatment steps leading to the AFM images depicted in Figure 9 are summarized in Table 4.

Table 4: *Steps of treatment leading to AFM images shown in Figure 9.*

	Wafer (a)	Wafer (b)	Wafer (c)	Wafer (d)
1. Wiping with tissue	×			
2. Ultrasonic bath (toluene)	×	×	×	×
3. Ultrasonic bath (ethanol)				×
4. Rinsing and drying	×	×	×	×
5. Wiping with tissue				×
6. Ultrasonic bath (toluene)				×
7. Ultrasonic bath (ethanol)			×	×
8. Rinsing and drying			×	×

When trying to determine the surface coverage from the AFM images, the differing depths of the scratches make an exact adjustment of the depth above which island points are identified almost impossible. The reason for this fact is that the second derivative of the height sum curve of the AFM images as used for determination of the surface coverage[82] does not show a clear minimum for the calculation of the island points.

Thus, a new method for the post-deposition cleaning treatment, leading to fewer scratches on the surface, was searched. At first simply the wiping with the drenched tissue was cancelled. Figure 9b shows a wafer treated in this manner. A large number of agglomerates (small dotted white features) can be seen. Such features also disturb the motion of the AFM tip during scanning leading to white horizontal lines in the AFM images. Thus, wafers treated in this manner were undergone a further cleaning step. They were sonicated in a glass beaker filled with ethanol and then blown dry in a nitrogen stream. The result can be observed in Figure 9c, which is an image of the same wafer as depicted in Figure 9b. It can be seen that the number of agglomerates is strongly decreased and therefore no white horizontal lines can be found in this image. In fact, as sonication in ethanol dissolves most of the agglomerates that were not removed from the surface by sonication in toluene indicates that most agglomerates are of hydrophilic nature.

In the case of Figure 9c, the two subsequent sonications resulted in a clean wafer suitable for computation although white dots of residual impurities can be observed even in this image. Thus, a treatment procedure was introduced combining ultrasonic treatment in toluene and ethanol and wiping of the wafers. After the first

cleaning step, the wafers were dried in a nitrogen stream. Then, they were wiped with a tissue drenched in toluene and again sonicated twice. Finally, the process was finished by drying the wafers in a nitrogen jet. A typical AFM image produced in this manner is depicted in Figure 9d. It can be seen that wiping subsequent to the drying process does not lead to scratches on the surface. This is most probably due to the drying process leading to some kind of stabilization of the ODS film.

7.2 The Influence of the Water Concentration on the Deposition Behavior

Figure 10 show s a comparison of four AFM images depicting the influence of the water concentration on the ODS growth for a temperature of 20°C and an adsorption time of 15 s.

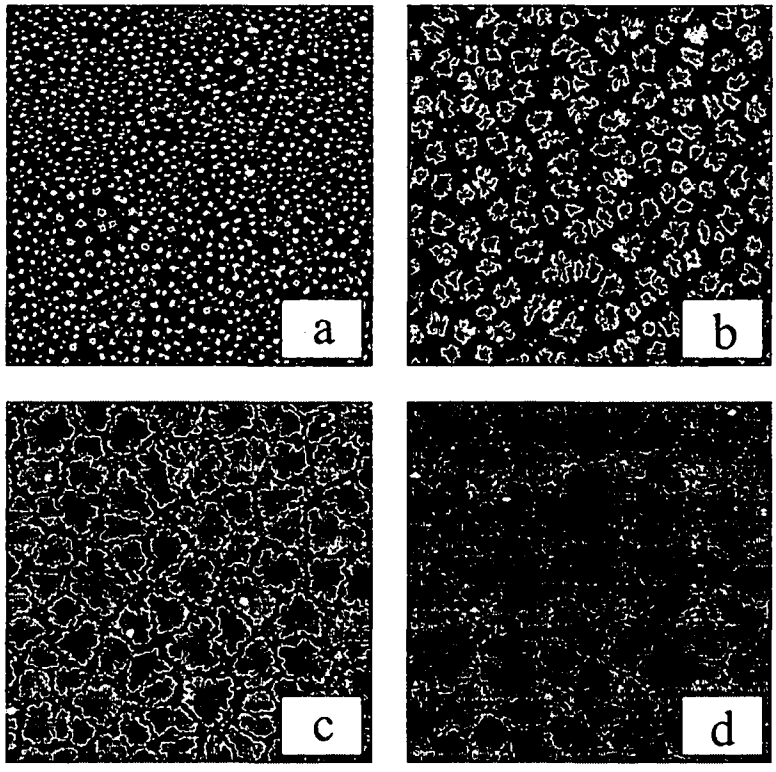

Figure 10: *AFM images of ODS on silicon demonstrating the influence of the water concentration in the solvent: T = 20°C, c(OTS) = 1 mmol/L, the adsorption solutions were matured for 10 min, adsorption time = 15 s;* ***(a)*** *$c(H_2O)$ = 10.2 mmol/L;* ***(b)*** *$c(H_2O)$ = 12.7 mmol/L;* ***(c)*** *$c(H_2O)$ = 14.2 mmol/L;* ***(d)*** *$c(H_2O)$ = 16.9 mmol/L, image sizes: 25 x 25 µm².*

It can be seen that an increase of the water concentration of only 7 mmol/L strongly increases the island size and surface coverage under otherwise identical conditions. Figure 11 shows that at 30°C ordered island growth does not take place anymore at a water concentration of 15 mmol/L, whereas at 18 mmol/L sub-monolayer islands characteristic for self-assembly growth are still observed.

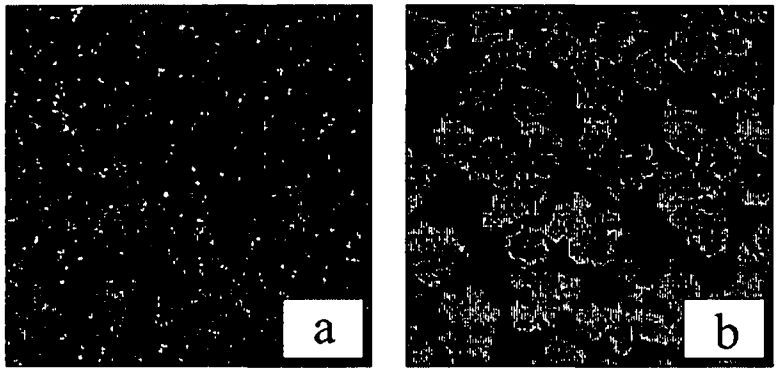

Figure 11: *AFM images of the growth of ODS on silicon at a temperature of 30°C: c(OTS) = 1 mmol/L, the adsorption solutions were matured for 10 min;* ***(a)*** *$c(H_2O)$ = 15.0 mmol/L, adsorption time = 10 s;* ***(b)*** *$c(H_2O)$ = 18.0 mmol/L, adsorption time = 5 s; image sizes: 5 x 5 µm².*

Figure 12 shows the ellipsometric surface coverage of ODS films as a function of the deposition time. Four different water concentrations (5.2, 7.3, 10.4 and 14.4 mmol/L) were investigated. Since the temperature was not controlled during these experiments, the ambient temperature of 28°C led to distinctly prolonged adsorption times. In general, increasing deposition rates at higher water concentrations were observed. The solid lines indicate calculated Langmuir-adsorption curves, which are mostly utilized when fitting kinetic data from SAM deposition, although necessary requirements (e.g. only one adsorbed species, no interaction between the adsorbed molecules, adsorption centers energetically equal) are not really fulfilled. Thus, these curves should mainly serve as a guide for the eye. The simple approach for Langmuir kinetics is that the rate of the coverage increase is proportional to the uncovered space on the surface.

$$\frac{d\Theta}{dt} = k * (1 - \Theta)$$

which leads to

$$\Theta = 1 - e^{-k*t}$$

wherein Θ is the surface coverage, t is the adsorption time, and k is the adsorption constant. In Figure 12 the surface coverages are given in %, and are derived from the ratio between ellipsometric films thickness and nominal film thickness of a full monolayer (2.6 nm).

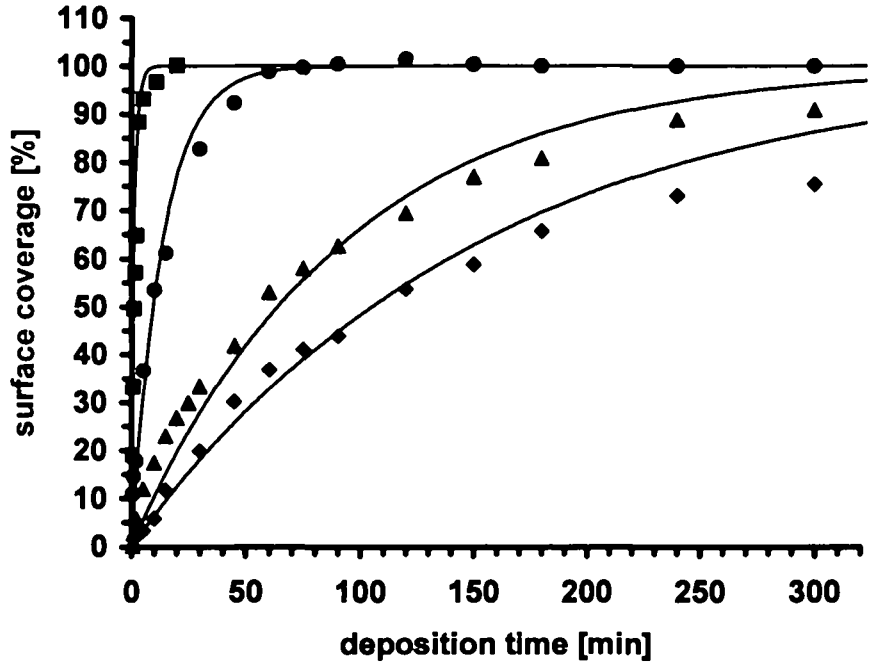

Figure 12: *Adsorption kinetics of OTS on silicon for different water concentrations: ellipsometric surface coverage vs. deposition time: c(OTS) = 1.0 mmol/L, maturation time of the precursor solution = 10 min, deposition temperature T = 28°C; water concentrations: (■) c(H_2O) = 13.4 mmol/L; (●) c(H_2O) = 10.4 mmol/L; (▲) c(H_2O) = 7.3 mmol/L; (♦) c(H_2O) = 5.2 mmol/L. The solid lines show a fit of the data according to a Langmuirian adsorption model.*

In general increasing adsorption rates with increasing water concentration can be observed. For all four cases it has been found that in the initial phase of adsorption (up to approximately 1 hour for the water concentrations of 5.2 and 7.3 mmol/L) the ellipsometric surface coverages are higher than the Langmuirian fit. Such an increased adsorption rate compared to the model could be explained by adsorption of larger aggregates instead of individual precursor molecules, which is presumed in the model. In fact, it is known from other experiments that under certain conditions ordered aggregates do exist in the adsorption solution and that these are responsible for fast ordered island growth particularly in the beginning of the adsorption process (chapters 7.3 and 7.4). Since the temperature for the experiments shown in this section was rather high (28°C), only for the highest water concentration of 13.4 mmol/L, AFM images showed an indication for ordered island growth via adsorption of larger aggregates from solution. Figure 13 shows AFM images of this series. In general, islands are found to increase in number in the course of time.

Between the islands smaller aggregates increasingly account for the overall surface coverage, until full monolayer coverage is reached.

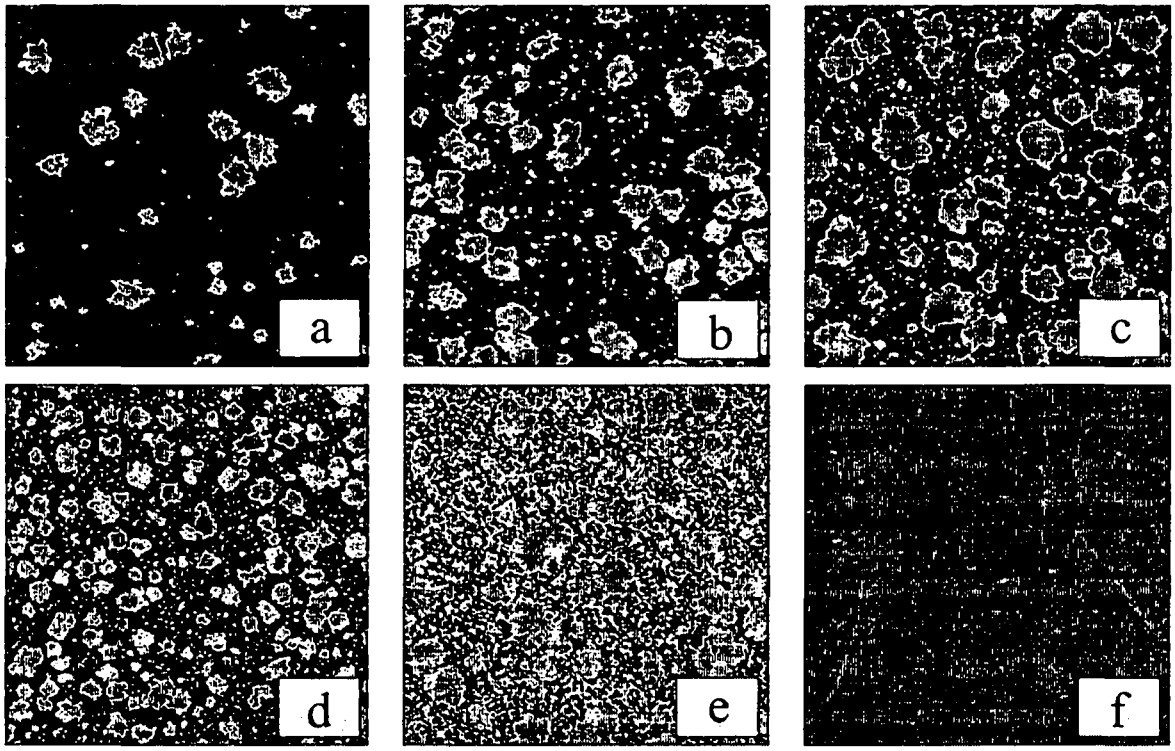

Figure 13: *AFM images of the growth of ODS on silicon at a temperature of 28°C: one of the kinetic series depicted in Figure 8, c(H_2O) = 13.4 mmol/L, c(OTS) = 1 mmol/L, the adsorption solutions were matured for 10 min, adsorption times:* ***(a)*** *t = 20 s,* ***(b)*** *t = 40 s,* ***(c)*** *t = 60 s,* ***(d)*** *t = 90 s,* ***(e)*** *t = 300 s,* ***(f)*** *t = 1200 s; image sizes: 4 x 4 µm².*

In all other cases AFM images revealed uniform growth. An example is shown in Figure 14.

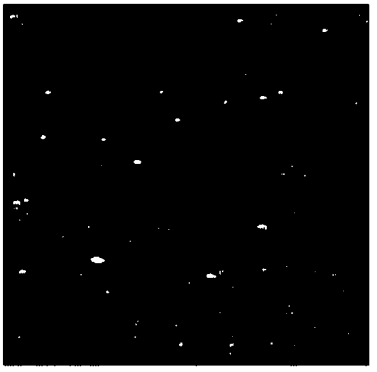

Figure 14: *AFM image of OTS adsorption on silicon at a temperature of 28°C: c(H_2O) = 5.2 mmol/L, c(OTS) = 1 mmol/L, the adsorption solutions were matured for 10 min, adsorption time = 15 min, image size: 4 x 4 µm².*

Nevertheless, the higher surface coverages in the first phase of adsorption, compared to the model, can still be explained by adsorption of oligomeric species which are too small, however, to achieve ordered growth observable by AFM. In the final phase of adsorption, the measured coverages are lower than suggested by the model, of course except for the region of full monolayer coverage in case of water contents of 10.4 and 13.4 mmol/L. This can be explained by hindered adsorption due to disordered attachment of precursors in the initial phase. Thus, full monolayer coverage can only be achieved, if reorientation of already adsorbed species in an ordered manner takes place. For the lower water concentrations of 5.2 and 7.3 mmol/L full monolayer growth cannot be achieved anymore due to high disorder in the films. In order to reach a substantial degree of order for such low water concentrations significantly lower temperatures than 28°C would be required. The influence of the complex interplay between water content and temperature on the ordering and growth behaviour of alkylsiloxane self-assembled monolayers will be addressed in chapter 7.4.

7.3 The Influence of the Temperature on the Deposition Behavior

Figure 15 shows first results of kinetic studies of the deposition of OTS on silicon using the temperature control unit described in the experimental part of this work. With this control unit kinetic investigations were performed at temperatures of 5°C and 20°C. The water concentration in these experiments was 13.1 mmol/L. Surface coverages were obtained from ellipsometry. The data points shown in Figure 15 are mean values of six different wafers treated in the same manner. The solid lines indicate langmuirian curves (approximated for the ellipsometric values as described above).

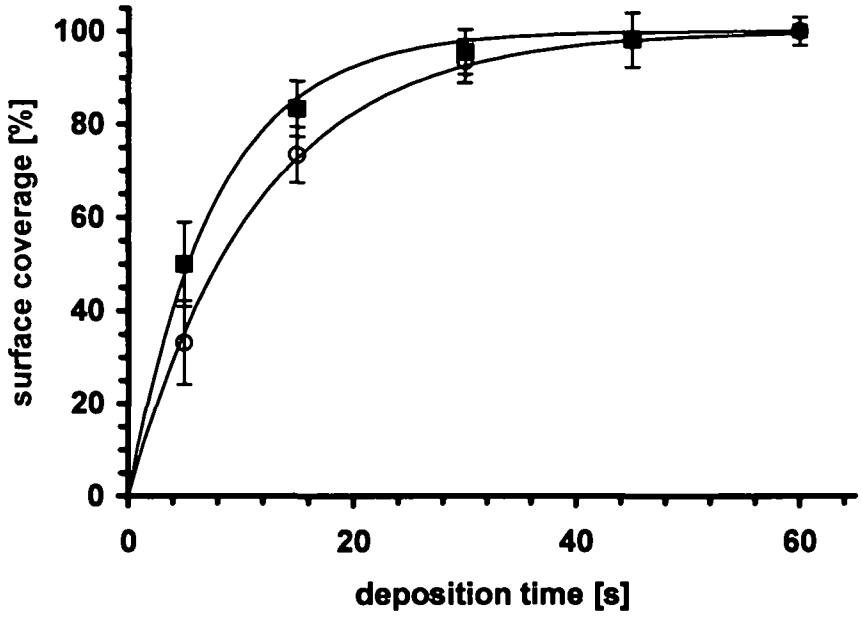

Figure 15: *Kinetic studies of the deposition of OTS on silicon: Ellipsometric surface coverages versus deposition time; c(H_2O) = 13.1 mmol/L, c(OTS) = 1.0 mmol/L, maturation time of the precursor solution = 10 min; (■) T = 20°C; (○) T = 5°C.*

It can be clearly seen that deposition is faster at 20°C and therefore formation of full monolayer coverage is obtained earlier. Although full monolayer coverage can be obtained at both temperatures, especially at shorter deposition times of 5 or 15 s distinct differences in surface coverage can be observed.

Figure 16 shows AFM images of the samples corresponding to the data depicted in Figure 15. In general two main features can be found. Firstly, it can be seen that at short deposition times the islands show a pronounced dentritic shape. With proceeding adsorption, the free space between the islands is filled up and therefore the edges of the islands become smoother. Secondly, at the lower temperature larger islands with more fractal-like shapes can be identified. This is a clear indication for reduced mobility of the adsorbed molecules. Moreover, at the lower temperature besides the fractal-like islands smaller circular dots can be observed particularly for a deposition time of 5 s.

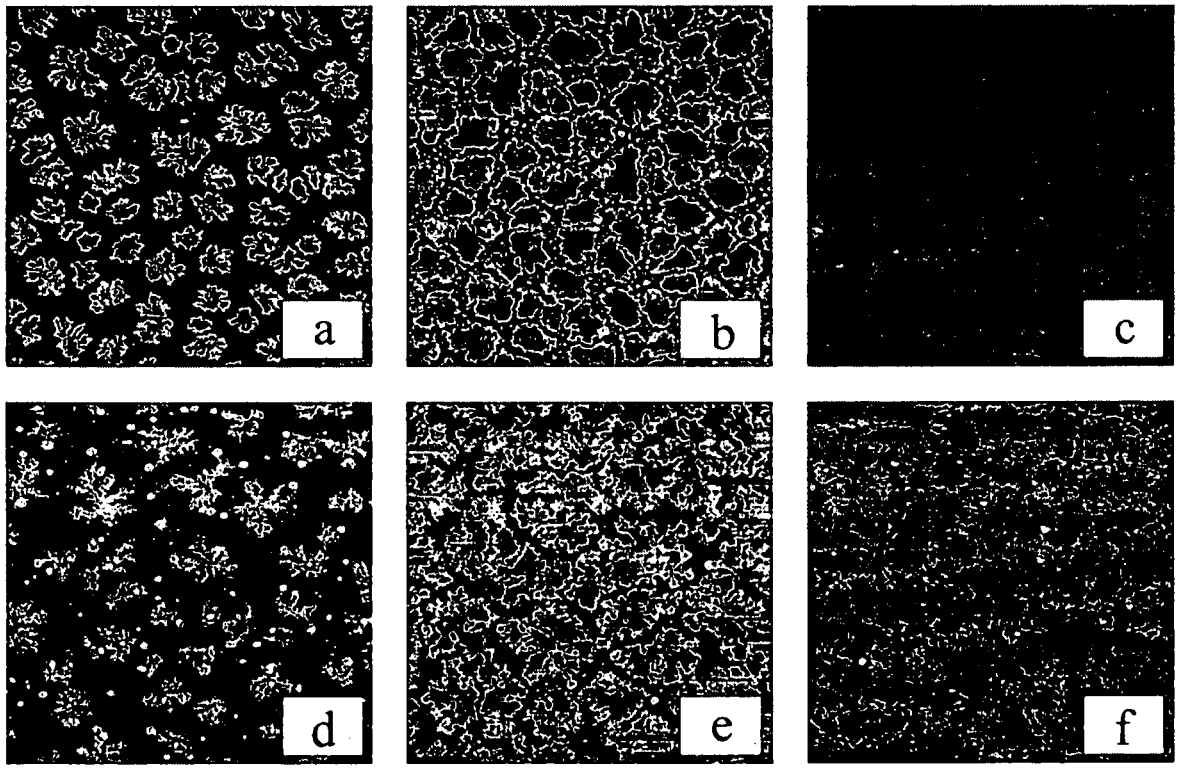

Figure 16: *AFM images of the growth of ODS on silicon: c(H_2O) = 13.1 mmol/L, c(OTS) = 1.0 mmol/L, maturation time of the precursor solution = 10 min, deposition temperatures T and deposition times t:* ***(a)*** *T = 20°C, t = 5 s;* ***(b)*** *T = 20°C, t = 15 s;* ***(c)*** *T = 20°C, t = 30 s;* ***(d)*** *T = 5°C, t = 5 s;* ***(e)*** *T = 5°C, t = 15 s;* ***(f)*** *T = 5°C, t = 30 s; image sizes:* ***(a)***, ***(b)***, ***(d)*** *–* ***(f)*** *20 x 20 µm², (c) 4 x 4 µm².*

This finding is of significant importance for the growth mechanism of ODS films on silicon and will therefore be discussed separately in chapter 7.3.5.

As these results suggested a distinct influence of the deposition temperature depending on the water concentration, experiments with fixed water concentrations

of 8, 10, 12, 15, and 18 mmol/L and varying deposition temperature were carried out. In the following sections results from three of these series (10, 12, 15 mmol/L) are shown in detail, each of them highlighting a specific aspect of the influence of the deposition temperature. In the sections 7.3.1 to 7.3.3 the following aspects of the role of the temperature will be addressed: the interplay between the deposition time and the temperature (section 7.3.1), the comparability between ellipsometry and AFM results (section 7.3.2), and the changes in island formation including island shapes and island sizes (section 7.3.3). For sake of completeness the results of the studies at 8 and 18 mmol/L are summarized in section 7.3.4.

7.3.1 Experiments at a Water Concentration of 10 mmol/L

For a water concentration of 10 mmol/L the influence of the deposition temperature on the growth behavior was investigated at three different immersion times (15, 30, and 60 s). Data points were recorded with temperature intervals of 2°C except for the series with a deposition time of 60 s (2.5 or 5°C). Figure 17 shows ellipsometric coverage values for all three deposition times versus deposition temperature. All data points represent mean values obtained from two individual wafers consecutively immersed in different reaction solutions. Expectedly, with increasing duration of immersion the resulting coverage also increased. Interestingly, increasing temperature initially yielded in approximately constant or slightly increasing coverage until a weak maximum was reached at 8°C for deposition times of 15 and 30 s, and 10°C for a deposition time of 60 s. Thereafter, a distinct decrease in coverage was observed in all cases.

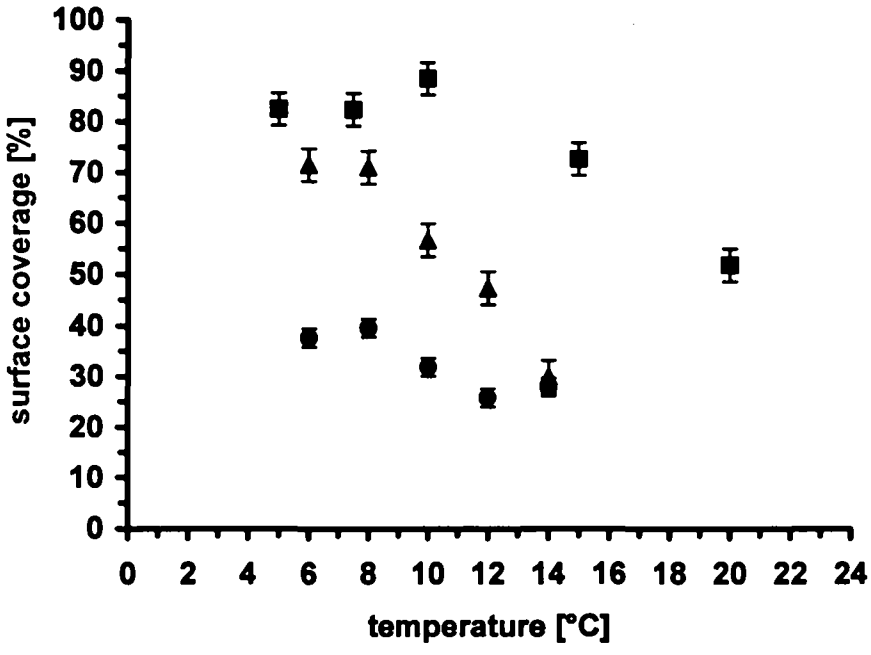

Figure 17: *Ellipsometric surface coverage versus deposition temperature: c(OTS) = 1.0 mmol/L, c(H_2O) = 10 mmol/L, maturation time of the precursor solution = 10 min, adsorption times are (■) t = 60 s, (▲) t = 30 s, and (●) t = 18 s.*

Figure 18 shows AFM images of OTS adsorption on silicon. The adsorption temperature was 10°C in all cases and the wafers were immersed 18 s in case of the images in Figure 18a and b, and 60 s in case of the images in Figure 18c and d. The corresponding ellipsometric coverage values can be seen in Figure 17. In principal, the wafer obtained from 18 s immersion exhibits jagged, fractal-like islands, whereas the wafer with an adsorption time of 60 s shows densely packed islands that are mostly coalesced due to the high coverage.

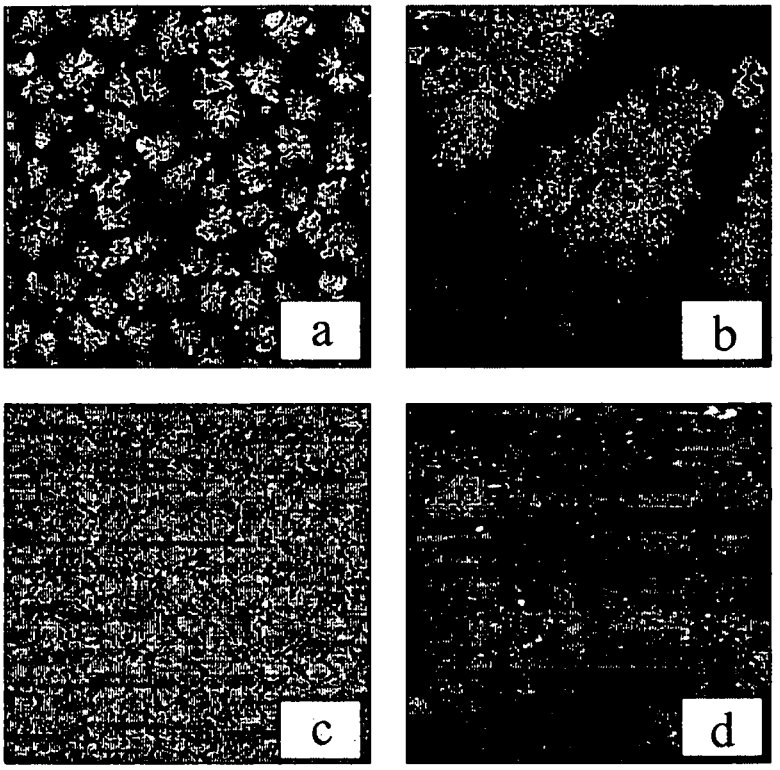

Figure 18: *AFM images of the growth of ODS on silicon: c(H_2O) = 10 mmol/L, c(OTS) = 1.0 mmol/L, maturation time of the precursor solution = 10 min, deposition temperature = 10°C, deposition times are* ***(a)****,* ***(b)*** *t = 18 s;* ***(c)****,* ***(d)*** *t = 60 s; image sizes:* ***(a)****,* ***(c)*** *25 x 25 µm²;* ***(b)****,* ***(d)*** *5 x 5 µm².*

In order to obtain quantifiable images the immersion times have to be adjusted to achieve medium surface coverage. On the one hand, short deposition times necessary for low coverages are leading to strong fractal shapes of the islands, which are poorly analyzable with respect to coverage and island size by AFM. Furthermore, ellipsometry utilizing the four-phase model (see chapter 6.2) yields best results with full monolayers, and thus, the higher the coverage the more accurate is the ellipsometric value. Moreover, especially at higher water concentrations the very short deposition times required for low coverages are hard to exactly control and therefore derogate reproducibility. On the other hand high coverage leads to increasingly inaccurate AFM image evaluation due to the molecular adsorbed species on the surface that are not detectable and due to problems in the differentiation of uncovered substrate and island surface. Moreover, in Figure 18d dark horizontal lines originating from an unsatisfactory flattening procedure indicate that AFM images are hardly flatable accurately in this coverage range due to the insufficient number of data points located on the uncovered substrate surface.

It turned out that coverages around 60% could be most accurately determined. Moreover, this stage of film adsorption is well located in the steep part of the growth curve, where pronounced changes upon variation of growth parameters can be expected – in contrast to the flat part of the curve running asymptotically towards full monolayer coverage.

On the basis of these considerations different deposition times were investigated for each water concentration. These preliminary experiments revealed that 60% coverage – corresponding to layer thicknesses of 1.5 to 1.6 nm – were most closely achieved under the conditions given in Table 5.

Table 5: *Combination of growth parameters leading to surface coverages of approximately 60%.*

water content [mmol/L]	temperature [°C]	deposition time [s]
8	2	30
10	5	30
12	10	15
15	15	10
18	20	5

7.3.2 Experiments at a Water Concentration of 12 mmol/L

Figure 19 shows the surface coverage as obtained by ellipsometry versus deposition temperature for a water concentration of 12 mmol/L. The data points represent mean values of four wafers consecutively immersed in different deposition solutions. As depicted in Table 5, an immersion time of 15 s was utilized for all wafers. Qualitatively, the shape of the curve is very similar to the results obtained at a water concentration of 10 mmol/L. However, the increase in coverage and the strong decrease after the maximum are even more pronounced and the maximum is shifted towards a higher temperature of approximately 13.5°C.

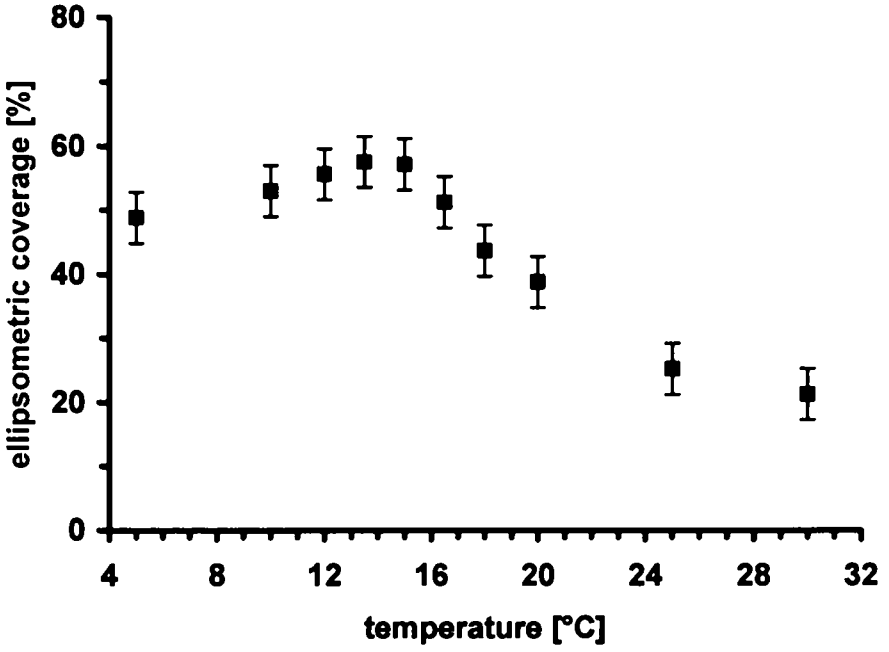

Figure 19: *Ellipsometric surface coverage versus deposition temperature: c(OTS) = 1.0 mmol/L, c(H_2O) = 12 mmol/L, maturation time of the precursor solution = 10 min, adsorption time = 15 s. Each data point represents the mean of four individual wafers.*

Figure 20 shows a comparison of the surface coverage obtained from ellipsometry and data evaluation of AFM images. Unlike the data depicted in Figure 19 each data point has been obtained from one individual wafer. Thus, differences between AFM and ellipsometry values can be related to the characteristics of the two methods. AFM values were determined from 25 x 25 µm² images.

In general, a good agreement between AFM results and ellipsometry can be seen and the plateau in coverage up to 15 °C can be verified in the AFM data. Three main aspects can be derived from the comparison of AFM and ellipsometry data. Firstly, at low temperatures AFM values are distinctly higher than coverages obtained from ellipsometry, whereas at higher temperatures (25°C and above) the picture is reversed. In the medium temperature range of 10 to 20°C a good agreement between AFM data and ellipsometry can be observed. These deviations can be explained by the fact that the AFM values are based on the detection of ordered sub-monolayer islands whereas the ellipsometric coverage represents the total amount of adsorbed material. In fact, this deviation is also a proof that film growth at elevated temperatures takes place via adsorption of individual molecules in a disordered

manner. As these individual molecules cannot be resolved by the AFM, due to large image sizes chosen to depict the islands, lower coverage values are yielded. This is demonstrated in Figure 21 and Figure 22.

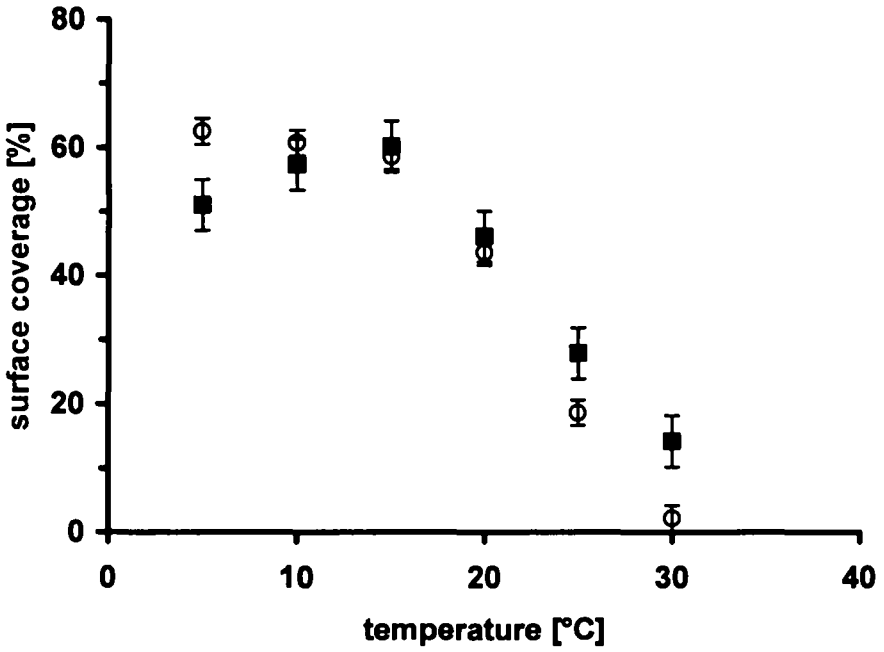

Figure 20: *Comparison of surface coverages obtained from ellipsometry (■) and AFM (○): c(OTS) = 1.0 mmol/L, c(H_2O) = 12.0 mmol/L, maturation time of the precursor solution = 10 min, adsorption time = 15 s.*

The somewhat higher AFM values at low temperatures can be explained by the comparatively high surface coverages and the strong fractal shape of the islands. In this case, convolution of the AFM tip with the surface geometry leads to elevated height values in the AFM images and, thus, to an overestimate in the calculated surface coverages. As an example Figure 21a shows a typical AFM image for which such an overestimate is usually obtained. Due to this artifact the maximum of the surface coverage as obtained by ellipsometry is not visible in the AFM data (Figure 20).

Figure 21 shows examples for wafers with good and bad agreement between AFM results and ellipsometry. The AFM images originate from wafers immersed at 5°C (Figure 21a), 15°C (b), 20°C (c), and 30°C (d). For the AFM data evaluation shown in Figure 20, 25 x 25 µm² images were utilized, however, in Figure 21 5 x 5 µm² images are depicted to emphasize the characteristics of the adsorbed features.

On the one hand, the images of Figure 21b and c contain islands with relatively smooth edges and very few small aggregates, and therefore the values from AFM evaluation agree well with the data from ellipsometry. On the other hand, nonconformance between ellipsometric and AFM coverage, deriving from overestimation due to the fractal shape of the islands and underestimation due to unordered growth of individual molecules, is apparent for the wafers depicted in Figure 21a and d, respectively.

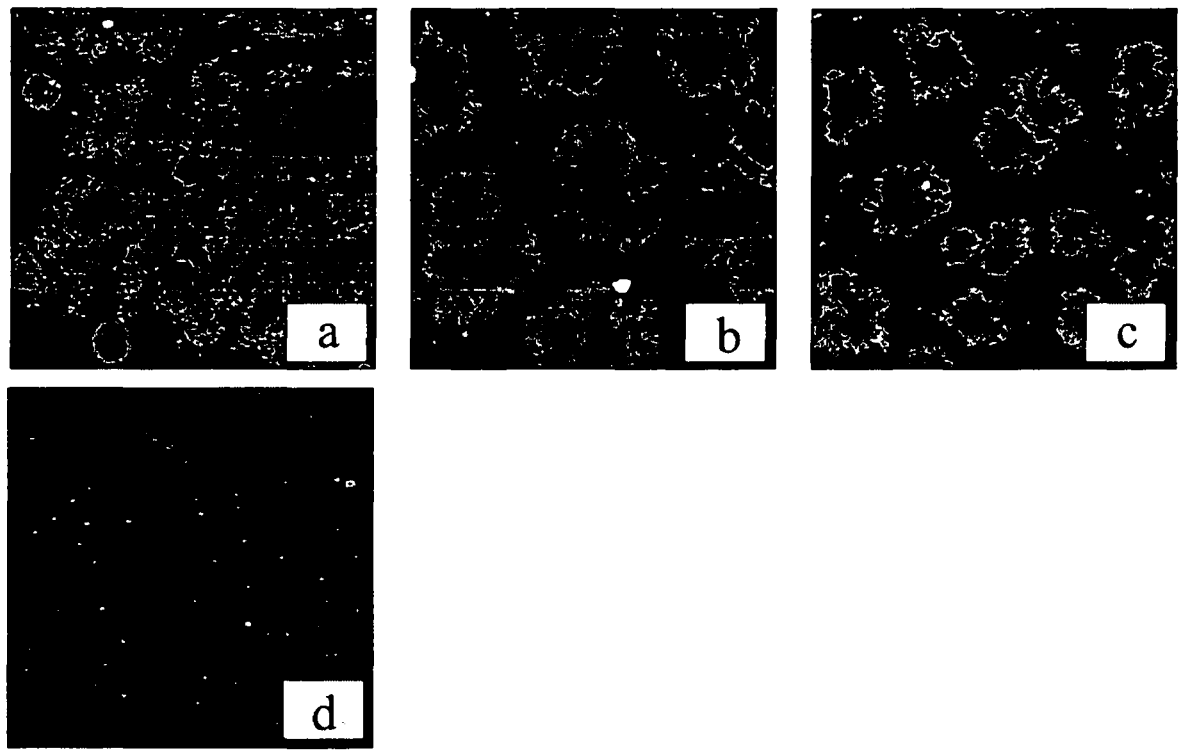

Figure 21: *AFM images of OTS adsorption on silicon demonstrating the reasons for fit and misfit between AFM- and ellipsometric coverages: c(OTS) = 1.0 mmol/L, c(H_2O) = 12 mmol/L, maturation time of the precursor solution = 10 min, deposition time = 15 s; deposition temperatures, AFM-, and ellipsometric coverage:* ***(a)*** *T = 5°C, AFM: 62.6%, ell.: 51.0%;* ***(b)*** *T = 15°C, AFM: 58.6%, ell.: 60.2%;* ***(c)*** *T = 20°C, AFM: 43.6%, ell.: 46.1%;* ***(d)*** *T= 30°C; AFM: 2.2%, ell.: 14.2%; image sizes: 5 x 5 µm².*

Figure 22 shows two wafers with similar surface coverage as obtained by ellipsometry (56.6% for the wafer depicted in Figure 22a, 53.5% for the wafer in Figure 22b). Whereas the AFM image presented in Figure 22a shows a coverage of 55.7% when evaluated with the custom-programmed software, data evaluation of the right image of Figure 22 results in a coverage of less than 1%. The coverage of the wafer depicted in Figure 22b mainly originates from disordered adsorption of

individual molecules or very small aggregates that are not resolved in the images and thus, coverage values obtained from AFM data evaluation are too low.

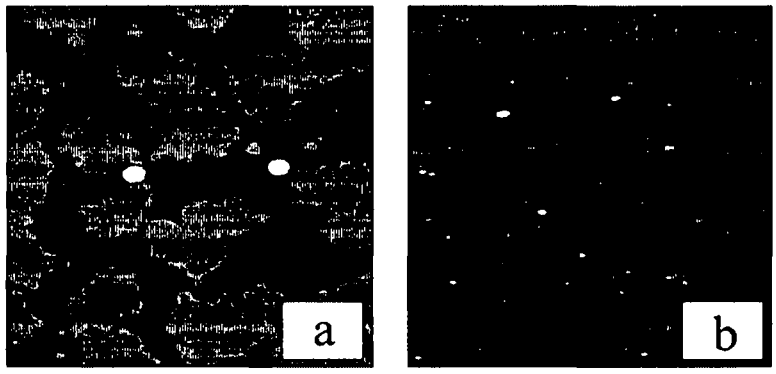

Figure 22: *AFM images of OTS adsorption on silicon with very similar surface coverages as measured with ellipsometry: coverages determined by AFM data evaluation differ widely:* ***(a)*** *$coverage_{Ellipsometry}$ = 56.6%, $coverage_{AFM}$ = 55.7%;* ***(b)*** *$coverage_{Ellipsometry}$ = 53.5%, $coverage_{AFM}$ < 1%.*

7.3.3 Experiments at a Water Concentration of 15 mmol/L

Next, the deposition of OTS has been studied in more detail on a quantitative basis in the temperature range from 10 to 30°C at a fixed water content of 15 mmol/L. In the first series of measurements, a temperature interval of 5°C was chosen. Since the corresponding results revealed that a weak maximum seemed to be apparent around 20°C, measurements in the region between 15 and 27°C have been repeated with temperature intervals of 2°C. Figure 23 shows a comparison of the surface coverages, as determined by ellipsometry and AFM, versus deposition temperature.

The diagram is based on the mean values obtained on two individual wafers and on the two measurement series mentioned above. After a slight increase in coverage up to a temperature of 21°C, a strong decrease can be observed. This strong decrease of the surface coverage is also evident in the AFM images shown in Figure 24. Figure 23 also demonstrates that the quantitative AFM data for the surface coverage obtained with the custom-programmed routine again agree very well with ellipsometric results.

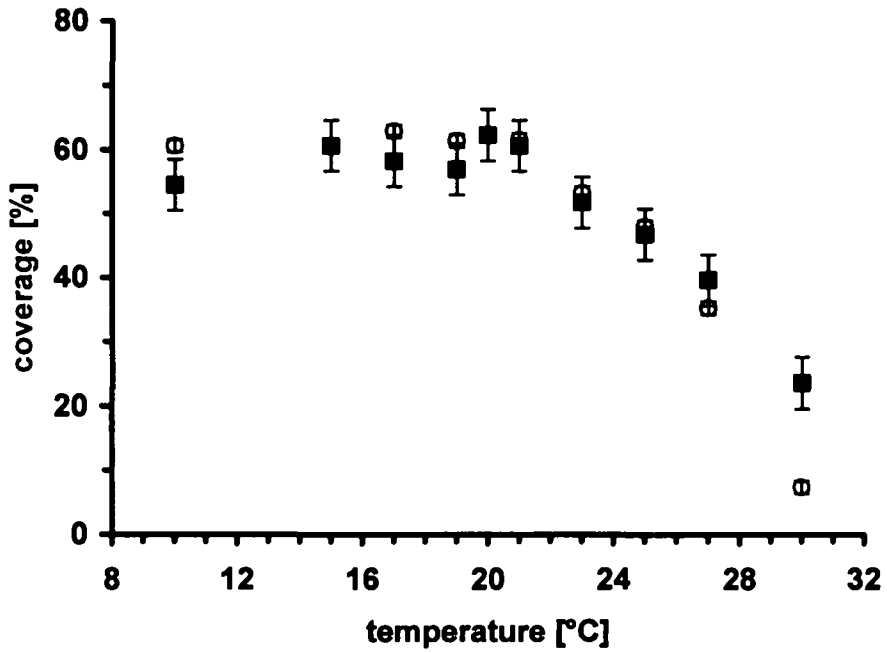

Figure 23: *Comparison of surface coverages obtained from ellipsometry (■) and AFM (○): c(OTS) = 1.0 mmol/L, c(H_2O) = 15.0 mmol/L, maturation time of the precursor solution = 10 min, adsorption time = 10 s.*

This good agreement confirms that the AFM images in Figure 24 are representative for the growth process given the fact that in ellipsometry the signal is averaged over a much larger area than in AFM.

Figure 24 shows a series of AFM images depicting the adsorption of OTS on silicon for varying temperatures from 10 to 30°C. The adsorption time was 10 s in all cases. A pronounced decrease of the island size with increasing temperature can be observed. At low temperatures large islands with diameters in a range of typically 2 to 4 µm and strong fractal shape are found. With increasing temperature the geometry of the observed islands more and more changes towards a circular geometry with comparatively smooth edges. This could be explained by increased surface mobility at higher temperatures. It should also be pointed out that at 30°C the islands are orders of magnitude smaller than at 10°C. They are only still visible in Figure 24h because a different size of the imaged field (5 x 5 μm^2 instead of 25 x 25 μm^2) has been chosen in that case.

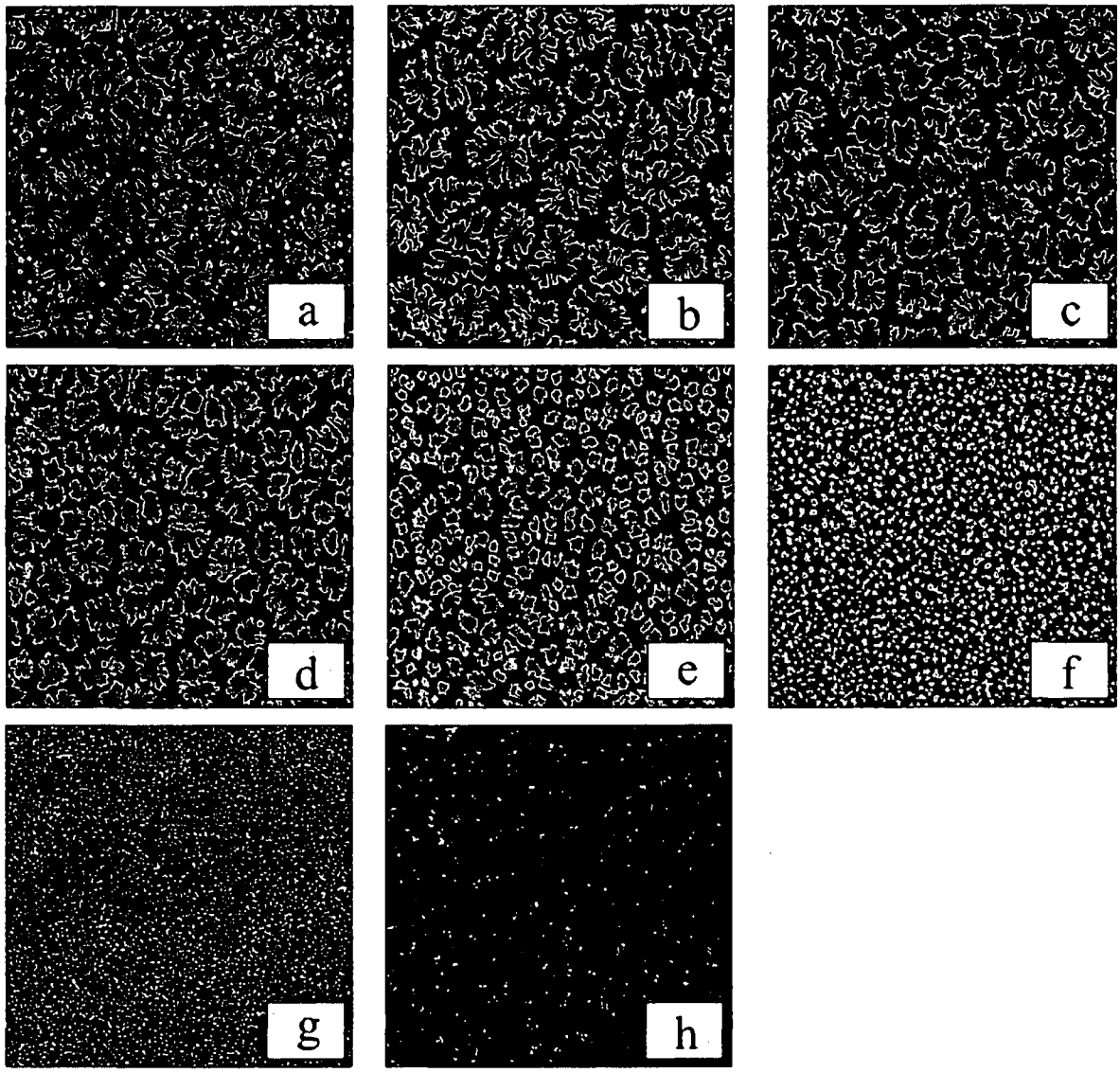

Figure 24: *AFM images of a series of adsorption experiments carried out at a water content of 15 mmol/L: image sizes:* ***(a)*** *–* ***(g)*** *25 x 25 µm², (h) 5 x 5 µm²; c(OTS) = 1.0 mmol/L, maturation time of the precursor solution = 10 min, deposition time = 10 s; deposition temperatures are* ***(a)*** *10°C,* ***(b)*** *17°C,* ***(c)*** *19°C,* ***(d)*** *21°C,* ***(e)*** *23°C,* ***(f)*** *25°C,* ***(g)*** *27°C,* ***(h)*** *30°C.*

Next, the AFM images were quantitatively evaluated with respect to the size of the islands which was accomplished according to the procedure described in chapter 6.5.8.

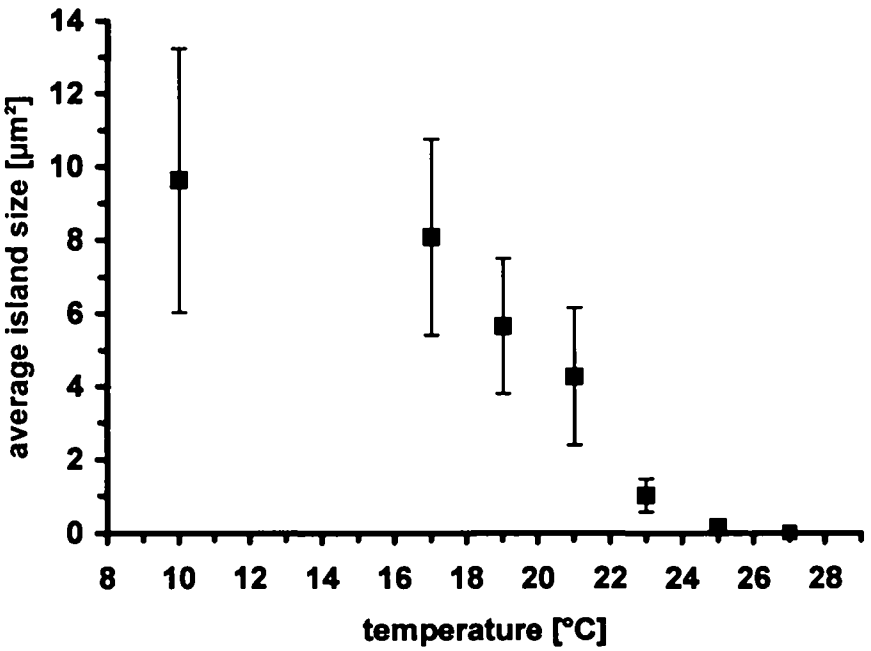

Figure 25: *Island sizes as a function of the temperature as determined from AFM images: c(OTS) = 1.0 mmol/L, c(H_2O) = 15.0 mmol/L, maturation time of the precursor solution = 10 min, deposition time = 10 s.*

Figure 25 shows the relation between island size, as obtained with the custom-developed software package, and adsorption temperature. The large "scattering bars" are due to the broad size distribution of the islands particularly at lower temperatures. It can be seen that the decrease in island size with increasing temperature, which is also apparent in the AFM images, is most pronounced in the temperature range around 20°C. Apart from the change in island size it is also interesting to note that at temperatures of 10°C (Figure 24a) or less a new type of islands occurs. Figure 24a clearly shows comparatively "small-dotted" features with diameters between 160 and 280 nm besides the large fractally shaped islands already addressed above. In chapter 7.3.5 these characteristic features are shown and discussed in more detail. It should be stressed that these small dots are excluded from calculation of the island sizes shown in Figure 25.

Figure 26 shows the results of a deposition series investigating the stability of aggregates formed in the deposition solution. Ellipsometric and AFM coverage values as well as island sizes are depicted as a function of time between the final agitation of the reaction vessel and the adsorption experiment. The data points

represent mean values of at least two individual wafers. After a first agitation subsequently to the addition of OTS all but two reaction vessels (data points at 10 min in Figure 26) were shaken a second time during the maturation time of the deposition solution (after 30 s, 5 min, 7.5 min, and 9.5 min, respectively).

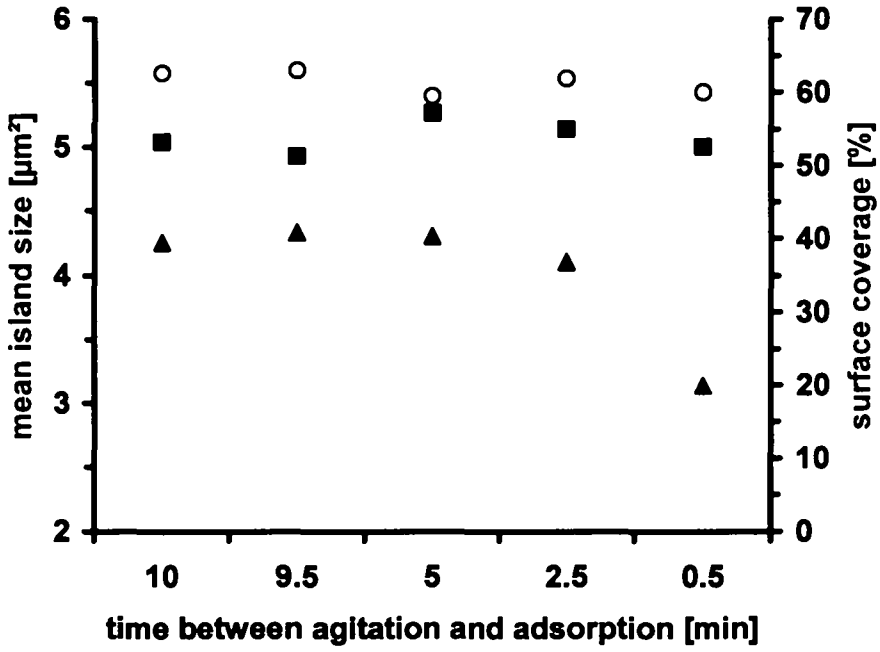

Figure 26: *The influence of agitation of the reaction vessels: mean island sizes (▲) obtained from deposition of OTS on silicon; c(OTS) = 1.0 mmol/L, c(H_2O) = 15.0 mmol/L, maturation time of the precursor solution = 10 min, deposition time = 10 s, deposition temperature = 20°C; the surface coverages were obtained from ellipsometry (■) and AFM data evaluation (○).*

It can be seen that an agitation of the reaction vessels shortly prior to the adsorption experiment leads to distinctly smaller islands. In fact, agitation even 150 s before the immersion of the wafer also leads to slightly decreased islands sizes. In contrast, the surface coverages as obtained from ellipsometry and AFM data evaluation are not affected by agitation of the reaction vessels. In fact, this was expected, since the deposition parameters were not varied and confirms that the changes of the mean island size are not related to changes of the surface coverage.

The organization process in solution leading to large islands most probably takes slightly more than 2.5 min at a water concentration of 15 mmol/L, since wafers immersed in the deposition solutions agitated 2.5 minutes prior to adsorption show

slightly decreased island size values compared to the wafers whose deposition solutions were allowed to rest for a longer period of time.

Figure 27 shows AFM images of wafers immersed at temperatures of 17°C, 19°C, and 21°C, respectively. The figure is divided into three segments, each depicting two wafers at one distinct deposition temperature. It can be seen, that for wafers immersed at the same deposition temperature different island sizes were found depending on whether or not the solutions have been agitated prior to adsorption. For each AFM image an island size distribution curve is depicted. These curves are Gaussian distribution curves received through mathematical approximation. At first sum curves of the island sizes with integration steps of 0.5 μm^2 were generated for all wafers. The islands that are intersected due to the image boundaries were left unevaluated, just as well as very small islands or agglomerates were. These data were modeled with sum curves through the least square fit method. Then, Gaussian distributions were determined through differentiation of the fitted sum curves. The wafers showed approximately identical surface coverages as obtained by ellipsometry and AFM (standard deviation 3.25% for the ellipsometric values, and 4.30% for the AFM values) but widely differing island sizes. This result can again be ascribed to the influence of the agitation of the reaction vessels. It can be seen that the distributions for the wafers with the larger islands are in all cases broader than the others which is in accordance with the decreasing lengths of the scattering bars with decreasing mean island sizes as seen in Figure 25.

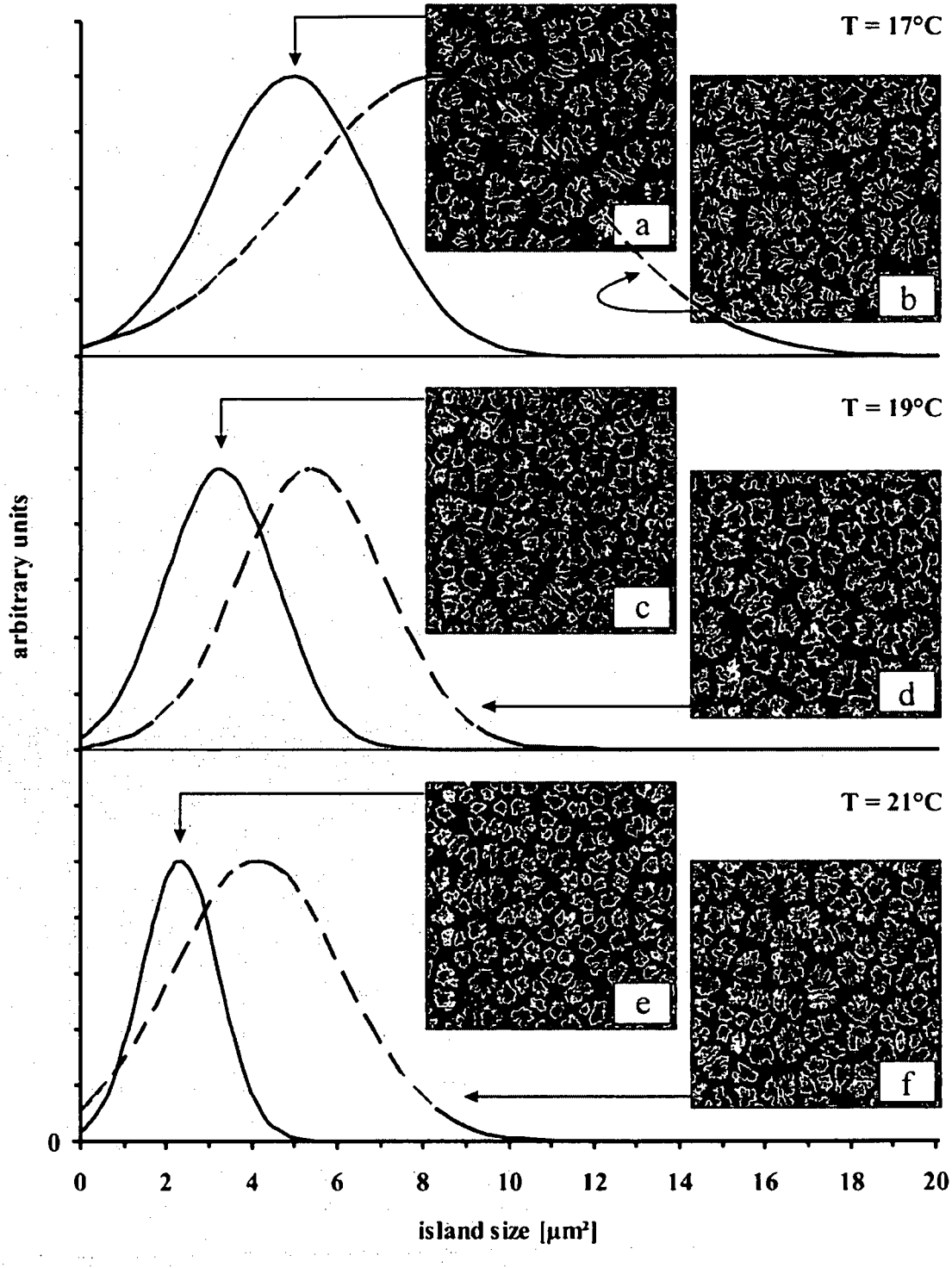

Figure 27: Island size distributions of ODS on silicon: Influence of the agitation of the reaction vessels: c(OTS) = 1.0 mmol/L, c(H_2O) = 15.0 mmol/L, maturation time of the precursor solution = 10 min, deposition time = 10 s; deposition temperatures: **(a)** and **(b)** 17°C, **(c)** and **(d)** 19°C, **(e)** and **(f)** 21°C; time between agitation and adsorption: **(a)**, **(c)**, and **(e)** 1.5 min **(b)**, **(d)**, and **(f)** 2.5 min; image sizes: 25 x 25 µm².

Table 6 shows the mean island sizes of the AFM images shown in Figure 27 versus time of the final agitation prior to the deposition experiment.

Table 6: *Deposition conditions and resulting mean island sizes for the wafers shown in Figure 27.*

wafer	deposition temp. [°C]	time between agitation and adsorption [min]	mean island size [µm²]	standard deviation [µm²]
Figure 27a	17	1.5	5.11	1.95
Figure 27b	17	2.5	8.17	2.77
Figure 27c	19	1.5	3.39	1.29
Figure 27d	19	2.5	5.48	1.66
Figure 27e	21	1.5	2.45	0.92
Figure 27f	21	2.5	4.44	2.01

These results suggest a previously unnoted strong influence of the processes in the deposition solution. Apparently, aggregates form in solution which are easily destroyed even by mechanical agitation of the reaction vessels and need a distinct period of time to form again. The following chapters (7.3.5 and 7.4) will show that such aggregates were in fact found utilizing dynamic light scattering measurements and are of main importance for the understanding of the whole deposition mechanisms.

7.3.4 Experiments at Water Concentrations of 8 and 18 mmol/L

For sake of completeness the results of the experiments performed with water concentrations of 8 and 18 mmol/L shall be mentioned here. In fact, these results will be further addressed in chapter 7.4. In short, with increasing temperatures the surface coverage also slightly increased until a maximum was reached (approximately 2 ± 2°C for a water concentration of 8 mmol/L, and 28 ± 2°C for a water concentration of 18 mmol/L, respectively) and thereafter it decreased distinctly. However, the great temperature differences to the ambient conditions for the series with 8 mmol/L water in toluene and the short adsorption times for the experiments

with 18 mmol/L made the experimental handling difficult and thus, the results are less explicit.

7.3.5 Adsorption Experiments at Low Temperatures

Figure 28 shows AFM images of ODS on silicon obtained from a wafer immersed at a temperature of 10°C. Three images with different image sizes are depicted in order to emphasize the appearance of dot-like islands typical for adsorption experiments at low temperatures.

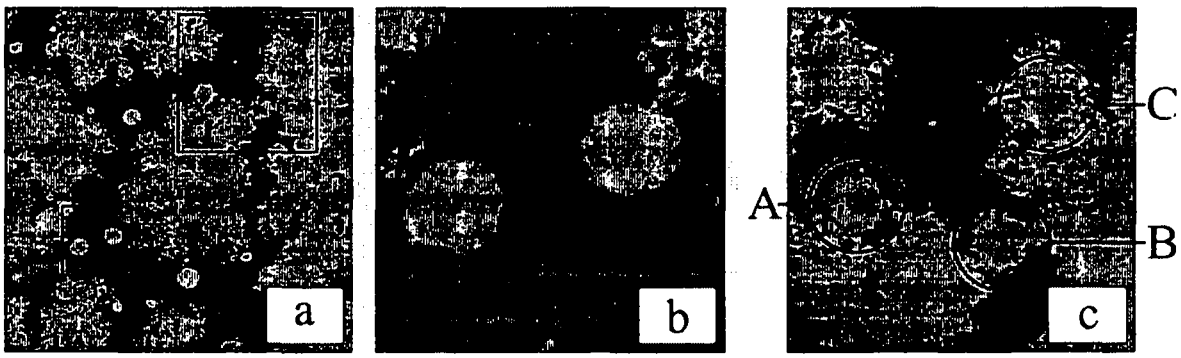

Figure 28: *AFM images of ODS on silicon adsorbed at a temperature of 10°C: c(OTS) = 1.0 mmol/L, c(H_2O) = 15 mmol/L, maturation time = 10 min.* ***(a)*** *Besides large fractally shaped islands smaller dot-like features can be observed. Image size: 5 x 5 µm^2.* ***(b)*** *Zoom of the lower left region in* ***(a)*** *showing isolated dots between the typical large islands. Image size: 1 x 1 µm^2.* ***(c)*** *Zoom of the upper right region in* ***(a)*** *showing dot-like features at different states of integration into the larger islands. Image size: 2 x 2 µm^2.*

Figure 28b shows a zoom of two isolated dots between the large fractal islands as marked with a square in Figure 28a. It is important to note that these dots exhibit an almost perfectly circular shape with very smooth edges. At the first glance this is surprising, because at low temperatures formation of such energetically favorable structures through diffusive rearrangement of individual molecules on the surface is very unlikely. In fact, the fractally shaped larger islands indicate that such a rearrangement actually does not occur. In order to shed more light on the origin of these dots, dynamic light scattering measurements of the precursor solution have been performed. These measurements revealed a very sharp size distribution of species in solution with a maximum at a hydrodynamic radius of 200 nm. From that we conclude that the dot-like islands in our AFM images are due to adsorption of

ordered species from solution. Since such species are only observed if sufficient water is available in the solution, we believe that these aggregates are most likely inverse micelles filled with water which will be discussed later in chapter 7.4. However, in principle also other structures cannot be excluded unequivocally. The discrepancy in size between the ordered aggregates in solution and the dots in the AFM images can be explained by disintegration of aggregates upon adsorption on the surface. Such a disintegration is supported by the low stability of these aggregates. In fact, there is evidence that they can already be destroyed by shaking of the solution as described in chapter 7.3.3. It should be noted that one such aggregate could supply enough material for approximately 10 dot-like islands with a diameter of ~ 250 nm. There is strong evidence that these features play a key role in the further adsorption process. Figure 28c shows three of these features located at the periphery of larger islands. Different stages of integration into the large islands can clearly be observed. In fact, feature C is already fully integrated into a larger island. This phenomenon can be seen even more clearly at a lower temperature of 5°C (Figure 29a). Figure 29a clearly shows that the large island consists of individual dots, while at 10°C (Figure 29b) these dots are fully coalesced and cannot be resolved anymore. It is also interesting to note that a decreasing density of the dots with increasing degree of coalescence has been observed. This could be explained by interface tension forcing the dots to partially disintegrate upon mutual contact.

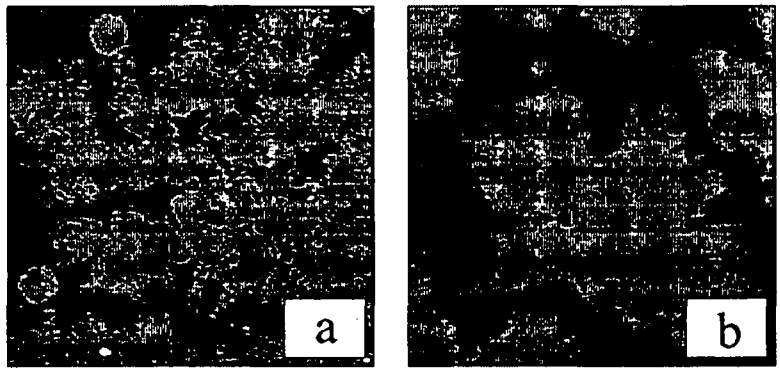

Figure 29: *AFM images of ODS on silicon adsorbed at a temperature of* ***(a)*** *5°C and* ***(b)*** *10°C: at 5°C it can clearly be seen that the larger islands are made up by coalescence of smaller dots; c(OTS) = 1.0 mmol/L, maturation time = 10 min, c(H_2O) = 12 mmol/L, deposition time = 15 s, Image sizes: 5 x 5 μm^2.*

The results described above are a key observation for interpreting the fast growth of large islands in the beginning of self-assembly adsorption. The main factor

governing the growth of the characteristic fractally shaped islands is the adsorption of larger ordered species which already exist in solution. Once adsorbed onto the surface their mobility is still high enough to coalesce and to integrate themselves into larger ordered units. Such coalescence is facilitated by the spatial vicinity of the small precursor islands which can be explained by their formation from one individual aggregate adsorbed from solution. In fact, many of the observed dots may already have been connected to each other upon formation. Since the mechanism of formation is not known exactly, it cannot be excluded that disintegration of the larger aggregates takes already place in solution triggered by the contact of the aggregates with the substrate surface. In any case, at low temperatures the mobility of these primary aggregates is sufficiently reduced making it possible to observe also isolated features as well as the transition to the typical larger islands well known in self-assembly processes. Above a temperature of approximately 23°C (for a water content of 15 mmol/L) the described ordered aggregates in solution almost completely disappear, as revealed by dynamic light scattering. Details on the light scattering experiments and their interpretation in terms of the growth mechanism of OTS on silicon can be found in chapter 7.4. Thus, growth in that temperature range must be dominated by adsorption of individual molecules and smaller species. This is manifested in a significantly reduced growth rate and the formation of smaller islands (See also Figure 24e-h). In the medium temperature range ordered species in solution still exist. However, in this temperature range their surface mobility is high enough in order to coalesce comparatively quickly. Thus, they cannot be observed in an isolated form anymore. Instead, less fractally shaped large islands can be seen (Figure 24c-d).

7.4 The Interplay between the Water Concentration and the Temperature

It has been shown that both water concentration and the temperature of the solvent are crucial parameters for the kinetics of the deposition reaction of ODS on silicon. Furthermore, for a given water concentration the deposition temperature decides between ordered and unordered monolayer growth to take place. On the other hand, for a fixed deposition temperature increasing the water concentration can change the growth mechanism leading to monolayer growth via ordered islands. Thus, the parameters cannot be considered separately but have to be seen in the interplay with each other.

Figure 30 shows that the growth of the film can be directed towards the desired structures by choosing appropriate combinations of water concentration and temperature. It should be noted that almost identical island sizes and coverages can be observed in Figure 30b, although the adsorption time was only 5 s compared to 15 s in Figure 30a.

Finally, it has to be kept clearly in mind that of course also the adsorption time is affecting the surface coverage. Since the deposition time does not lead to any changes in the growth regime, however, it has only been used as a regulating parameter for the surface coverage.

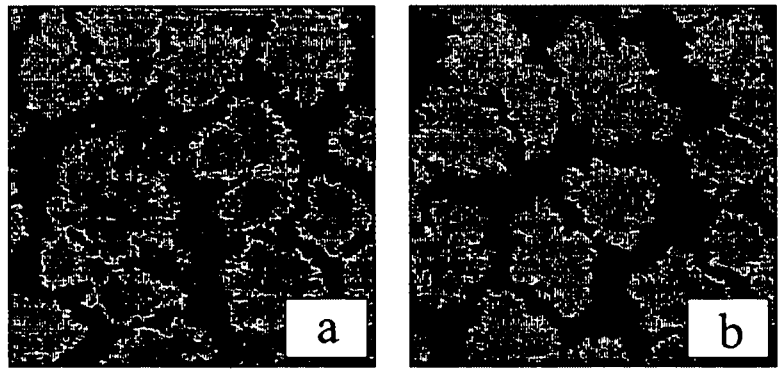

***Figure 30**: AFM images of the growth of ODS on silicon: c(OTS) = 1 mmol/L; the adsorption solution was matured for 10 min; **(a)** temperature = 13.5°C, c(H_2O) = 12 mmol/L, adsorption time = 15 s; **(b)** temperature = 28°C, c(H_2O) = 18 mmol/L, adsorption time = 5 s; image sizes: 5 x 5 μm^2.*

In Figure 31 characteristic temperatures (temperature exhibiting maximum surface coverage) are depicted as a function of the water concentration.

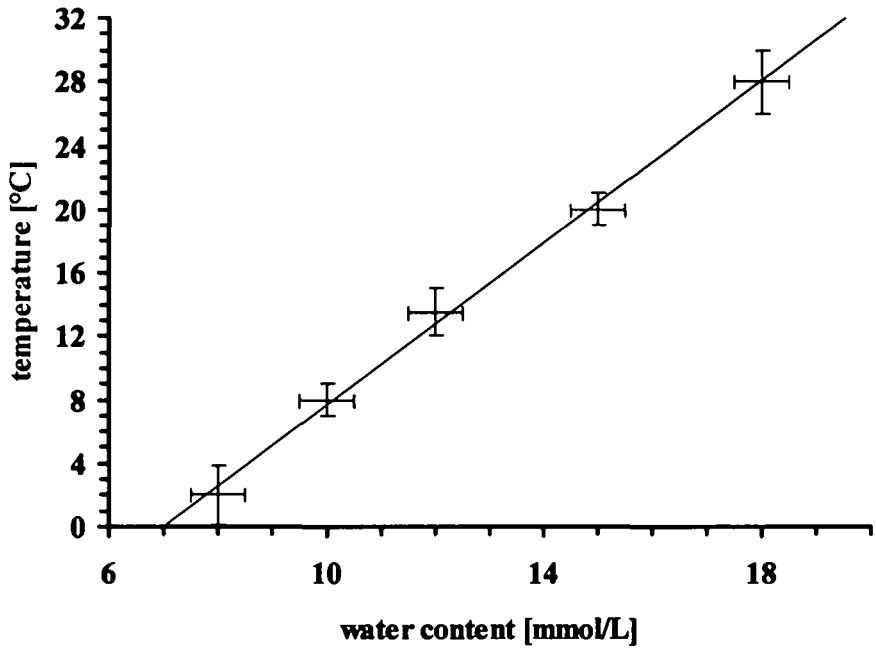

Figure 31: *Temperature of maximum surface coverage versus water concentration in the deposition solution: c(OTS) = 1 mmol/L, the maturation time of the precursor solution was 10 min in all cases, water concentrations and corresponding adsorption times: $c(H_2O)$ = 8 mmol/L, adsorption time = 30 s; $c(H_2O)$ = 10 mmol/L, adsorption time = 30 s; $c(H_2O)$ = 12 mmol/L, adsorption time = 15 s; $c(H_2O)$ = 15 mmol/L, adsorption time = 10 s; $c(H_2O)$ = 18 mmol/L, adsorption time = 5 s.*

Figure 31 clearly shows that the position of the maximum of the surface coverage is shifted towards higher temperatures with increasing water concentration (2.6 ± 0.4°C per mmol/L of water). Below the best fit straight line ordered monolayer growth via islands can be observed. The islands get larger with decreasing temperature. Above the line increasingly unordered growth takes place, islands get smaller until monolayer growth via islands is fading to an unordered growth.

It has to be noted that in all cases water is in great excess with respect to the amount of water required for complete hydrolysis of the OTS molecules. Thus, these results can only be explained through water-dependent ordering phenomena in the deposition solution. Therefore, the size distribution of the precursor species in the deposition solution has been investigated with dynamic light scattering (DLS)

experiments. For this purpose a cuvette has been filled with toluene containing a certain amount of water. Three experiments with water concentrations of 15, 12, and 6 mmol/L have been performed. The solutions were cooled down to a temperature of approximately 10°C. This temperature range was chosen in order to make sure to perform this experiment under conditions which normally lead to ordered island growth at elevated water concentrations of 12 and 15 mmol/L. The experiment with a water content of 6 mmol/L was carried out as a blank for the measurement. After the adjusted temperature had been reached, OTS has been added to the solvent. Immediately after the addition of OTS and mixing, first DLS data have been recorded. DLS peaks associated with larger species in solution have not been found. With increasing time of maturation DLS peaks indicating the formation of species with a hydrodynamic radius of 200 nm have been observed except for the lowest water concentration of 6 mmol/L. Surprisingly, this diameter was neither affected by the water concentration in the solution nor by the temperature (as revealed in further experiments described later on). It has been found, however, that the formation of these species proceeds at a higher pace at higher water concentrations and lower temperatures. The sharp size distribution of the aggregates in solution and the independence of the radius from water concentration and temperature may be explained by the fact that in all cases the water content is too low to enable the growth of larger inverse micelles. Even in case of our highest water concentration of 18 mmol/L, the molar ratio between water and OTS is 18:1 which is not sufficient to support growth of large inverse micelles with all OTS molecules available in solution. In fact, simple volume considerations show that about 3 times the water would be needed to bind all OTS molecules in inverse micelles with a hydrodynamic radius of 200 nm. However, such a high water concentration is not accessible experimentally, because the solubility limit of water in toluene is reached much earlier. Thus, only the smallest inverse micelles which can be formed under energetically favorable conditions are observed and the excess of OTS must be present in form of individual molecules. In this way the whole system obviously reaches its energy minimum.

Bunker et al.[59] have performed similar light scattering experiments with solutions of 1H, 1H, 2H, 2H-perfluorodecyltrichlorosilane (FDTS, c = 1 mmol/L) dissolved in isooctane with different water contents of 0.2, 0.8, and 4.3 mmol/L. In contrast to our results, they found objects in the solution which grew until a distinct hydrodynamic radius had been reached. Moreover, these authors found increasing

objects for increasing water contents. These results seem to be contradictory to our findings. It must be stressed, however, that these results are not directly comparable to ours, since a completely different system has been investigated at much lower water concentrations. Due to the fact that FDTS molecules exhibit a very weak mutual interaction, it is plausible that inverse micelles of FDTS can grow upon break-up and incorporation of further molecules. In contrast to that the stronger interaction between OTS molecules may stabilize our 200 nm structures and thus hindering further growth once formed from planar precursors.

Since the experiments described were not fully conclusive, it has been tried to reveal information on the concentration of the aggregates in solution by evaluation of the intensity of the DLS signal at various temperatures. At this point it should be mentioned that absolute concentrations of species can hardly be calculated from dynamic light scattering raw data. However, for unimodal size distributions the signal reaching the detector can be used to monitor changes in the concentration of the species with varying temperature, as can be seen in Figure 32. For these DLS measurements solutions have been prepared and allowed to mature for 10 minutes. Then they were slowly chilled in the DLS instrument starting from an initial temperature as seen in the curves in Figure 32. During this cooling run data have been recorded in intervals of approximately 1 minute. The data acquisition time was 10 s with 2 repetitions in all cases. After a plateau in the DLS signal had been reached the experiment has been continued with a heating run until again a constant DLS signal had been reached. The total time for both the cooling and the heating run was 1.5 hours for the solution with a water content of 15 mmol/L. The time for the heating run for the solution containing 12 mmol/L of water was 1 hour. Figure 32 shows the temperature dependence of the DLS signal for a water content of 15 mmol/L (Figure 32a) and 12 mmol/L (Figure 32b).

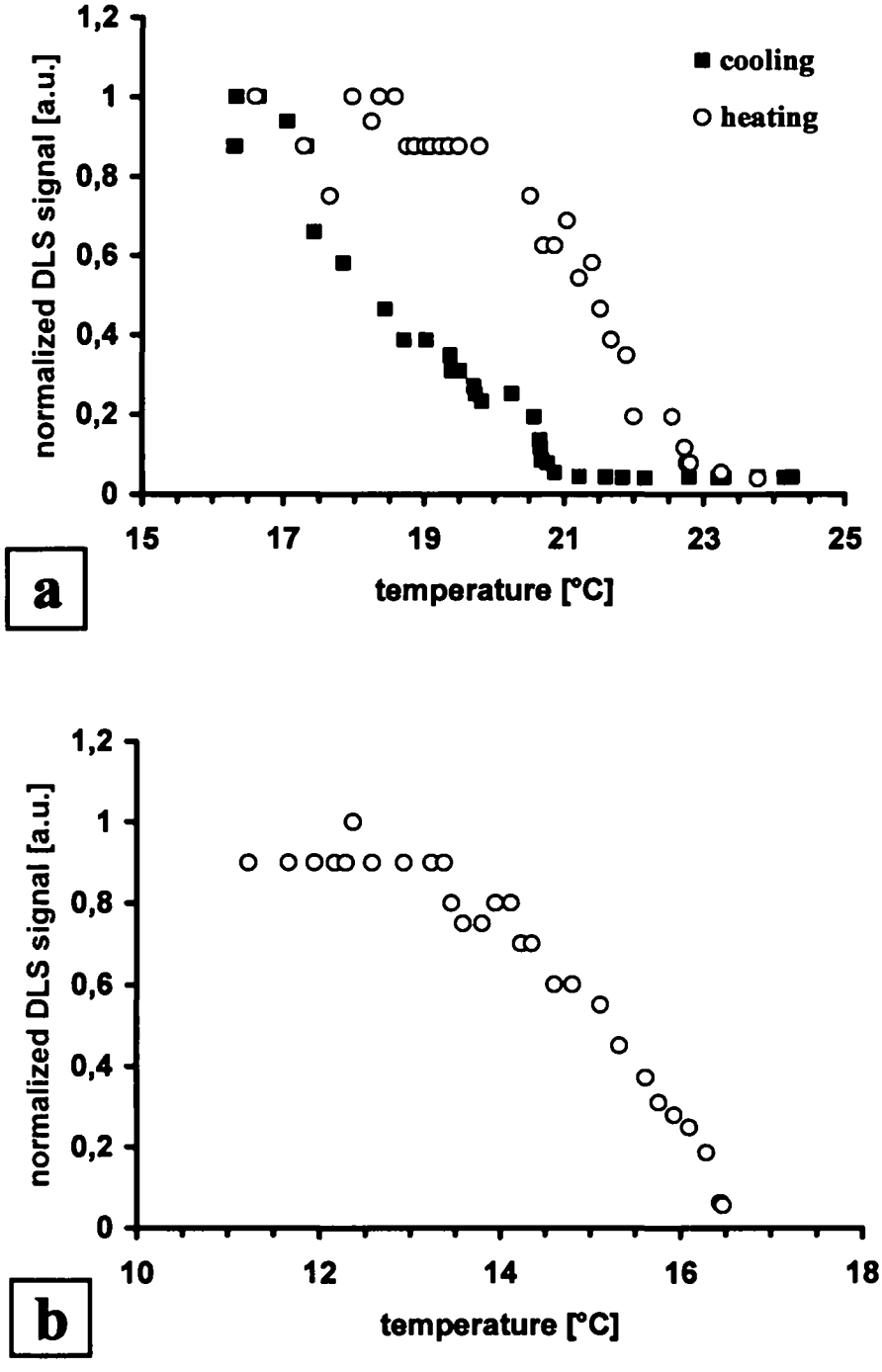

Figure 32: *Concentration of ordered aggregates in the precursor solution versus temperature: It should be noted that the data are depicted in form of the normalized raw signal of dynamic light scattering and that in all cases a unimodal size distribution with a constant hydrodynamic radius of 200 nm is observed. Quantification in terms of the absolute volume concentration of aggregates is not possible. c(OTS) = 1.0 mmol/L.* ***(a)*** *c(H_2O) = 15.0 mmol/L, the total time interval both for the cooling and the heating run was 1.5 h.* ***(b)*** *c(H_2O) = 12.0 mmol/L, the time interval for the heating run was 1 h.*

Clearly, in both cases a decrease of the concentration of aggregates with increasing temperature can be observed. It should again be emphasized that we are looking at aggregates with a constant diameter of 400 nm. Furthermore, a hysteresis loop can be observed indicating that the formation of the aggregates in the cooling cycle takes place at lower temperatures than the destruction of these aggregates in the heating cycle. At a higher water concentration of 15 mmol/L the curves are shifted towards higher temperatures by approximately 6°C. In both cases a characteristic temperature exists above which larger aggregates are not observed anymore. This temperature is 23°C for a water concentration of 15 mmol/L and 16.5°C for a water concentration of 12 mmol/L. Likewise a characteristic temperature exists below which the number of larger aggregates does not increase anymore. The value of this temperature is 11.5°C and 17°C for the water concentration of 12 and 15 mmol/L, respectively. The hysteresis in the cooling-heating loop can be explained by the fact that aggregates once formed are stabilized by intermolecular forces. Thus, their destruction requires a higher thermal budget than acceptable for the formation of these features from individual molecules.

To facilitate discussion of the described experiments, Figure 33 summarizes DLS results, ellipsometric film thicknesses, and island sizes in one diagram. The island sizes have been determined from AFM images as described in chapter 7.3.3. For reasons of lucidity DLS measurement and island sizes are only shown as fitted curves (least squares method applied on Gaussian sum curves in all cases) instead of individual data points. The results shown in Figure 33 have been obtained at a water concentration of 15 mmol/L. Apart from a shift on the temperature scale, data for other water concentrations look very similar (see also Figure 31).

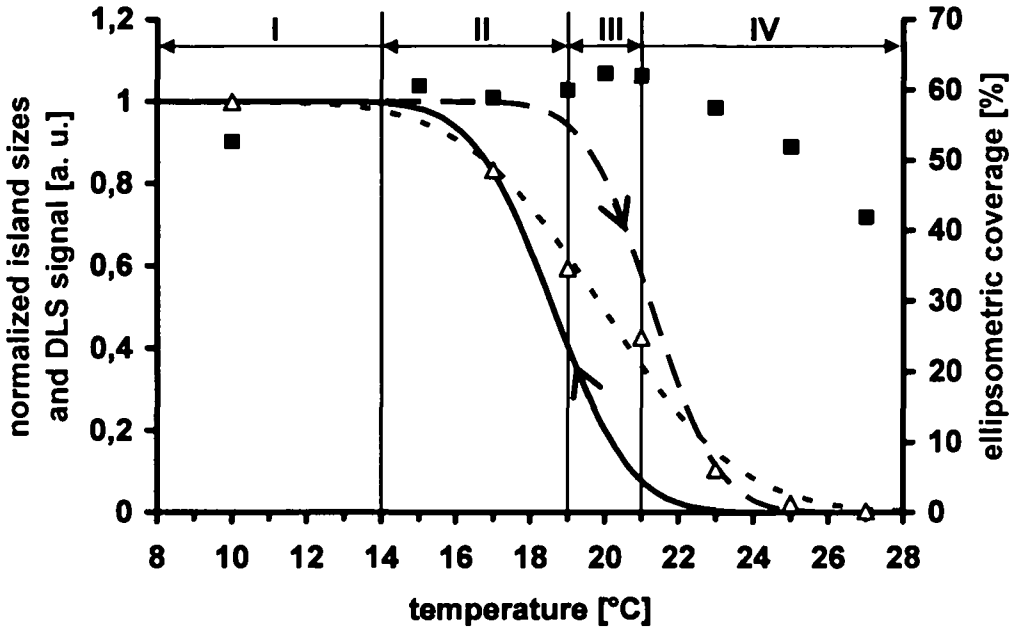

Figure 33: *Comparison of ellipsometric surface coverage (■), island size from AFM images (dotted line, Δ), and aggregate size in the precursor solution as obtained from dynamic light scattering (cooling run: solid line, heating run: dashed line): For sake of clarity DLS data are shown as modeled curves instead of individual data points. c(OTS) = 1.0 mmol/L, c(H_2O) = 15.0 mmol/L. For the adsorption experiments (i.e. island sizes and surface coverages) the maturation time of the precursor solution and adsorption time were 10 min and 10 s, respectively.*

Basically, four temperature regions can be identified in Figure 33. In region I, a plateau in the DLS signal can be observed. This indicates that in this region a maximum number of ordered aggregates in solution is present. From that it can be concluded that in this region growth is dominated by adsorption of these ordered aggregates leading to comparatively high growth rates and formation of large sub-monolayer islands which is actually confirmed by AFM and ellipsometry. In region II, the number of large aggregates in solution starts to decrease. At the same time the island size decreases and the ellipsometric surface coverage continues to slightly increase. In fact such a slight increase is already observed in region I. This indicates a slight increase of the growth rate with increasing temperature in that regions. This can be explained by increased precursor transport to the substrate surface due to higher diffusion rates. Such a diffusion-limited growth mode has already been reported for the adsorption of octadecylphosphonic acid from tetradydrofurane onto mica substrates, particularly for surface coverages below 60%[13]. The authors found that their data could not be fitted with an adsorption-limited model. Since the growth

rate still increases while both the island size and the number of aggregates in solution already decreases, it must be concluded that in this region growth by adsorption of individual molecules is becoming more and more important. In region III, a maximum of the surface coverage is reached and after that maximum a pronounced drop of the coverage can be seen. This phenomenon could be explained by transition from a diffusion-limited to an adsorption-limited growth process at higher temperatures. In fact, it has already been reported in literature that adsorption-limited models can describe the growth kinetics of self-assembled monolayers[83]. Furthermore, it must be noted that in the region of decreasing surface coverage the number of the large aggregates in solution is already strongly reduced. This means that there is a lack of nucleation centers on the surface which seems to be necessary for a fast self-assembly process. Thus, comparatively slow growth by adsorption of individual molecules becomes the dominating contribution. From that it can be concluded that the reduced growth rate is due to a combination of adsorption limitation and transition from growth via aggregates to growth via individual molecules. At even higher temperatures in region IV, large ordered aggregates in solution completely disappear and at the same time islands are not observed anymore in the AFM images. It should be pointed out, however, that in this region full monolayer coverage can still be achieved at prolonged adsorption times. Thus, the temperature in region IV of Figure 33, where the DLS signal drops to zero, must not be associated with the critical temperature (approximately 28 ± 5°C) found by Parikh et al.[61] above which full ordered monolayers cannot be obtained anymore regardless of the adsorption time. It must be kept in mind, however, that these authors have investigated a system largely different from ours (different solvent, different water content, substrate surface treated with water prior to adsorption of OTS).

8 Conclusion

The growth mechanism of self-assembled monolayers of alkylsiloxanes strongly depends on different deposition parameters. The work in this thesis has contributed to the understanding of the growth of octadecylsiloxane monolayer films on silicon with respect to the water concentration of the solvent and the deposition temperature.

For this purpose reproducible adjustment of the water concentrations in the solvent, toluene, has to be assured but was found to be non-trivial. Mixing of stock solutions of dry and humidified toluene exhibits bad reproducibilities, which are by far not sufficient to quantitatively investigate the kinetics of film formation for different experimental parameters. Therefore, a procedure was developed which utilizes direct doping of dry toluene in closely sealable lever-lid glasses with bidistilled, deionized water. Doping was performed in slight excess to the desired nominal water concentration to overcome problems regarding the low solubility and slow dissolution kinetics of water in toluene. In this way it was possible to adjust the water content in toluene with an accuracy of ± 3% without the need to wait for complete dissolution equilibrium which would require much more than one day.

The developed procedure is the basis for quantitative investigation of the self-assembly adsorption using ellipsometry and AFM. The influence of the water concentration in toluene was investigated at fixed deposition temperatures and yielded in increased growth rates for increases water concentrations, regardless whether ordered or unordered growth was observed. Adsorption kinetics for water concentrations between about 5 and 13 mmol/L were recorded. The obtained data were approximated through Langmuir adsorption curves. The achieved accuracy made it possible to reproducibly determine small deviations of measured adsorption rates from the Langmuirian adsorption model. These deviations could be explained in terms of adsorption of oligomeric species from solution in the early stage of the deposition and adsorption limitation due to disordered growth of the films in the later stage.

A good deal of this work was dedicated to the influence of the deposition temperature. Investigation of this crucial parameter was achieved by means of deposition experiments using toluene with five different water concentrations. Such experiments became possible by implementing a home-built temperature control unit into the glove box. In this way, adsorption of OTS from toluene with an accurately controlled water content was possible in a wide temperature range between 0 and 35°C. For all water concentrations the surface coverage was found to increase with increasing deposition temperature until a slight maximum or at least a plateau was reached. The temperature at which this maximum was observed was higher at higher water concentrations and was found to be between approximately 2°C (8 mmol/L) and 28°C (18 mmol/L). At temperatures above this maximum a distinct decrease in coverage was found. AFM images revealed ODS islands to become smaller with increasing temperature. Finally, at even higher temperatures a transition to unordered growth without noticeable islands was found in all cases.

At deposition temperatures considerably below the characteristic temperatures (e.g. 5°C for a water concentration of 12 mmol/L, 10°C for 15 mmol/L), the growth of the typical fractally shaped islands could be partially "frozen". In fact, it was possible to contribute to the understanding of the initial phase of the growth of ODS layers on silicon by means of adsorption experiments at low temperatures. This was the key to show that large islands, which are formed quickly in the initial stages of the growth process, are mostly built from dot-like islands that coalesce with increasing adsorption time.

Through DLS measurements of precursor solutions with different water concentrations and deposition experiments from these solutions, different modes and possibilities of octadecylsiloxane monolayer growth were highlighted. The results reveal that individual experimental growth parameters like the temperature and the water content in the precursor solution cannot be seen in an isolated manner. Rather the interplay between these parameters determines the growth mode in self-assembly processes. This may explain apparently contradictory reports claiming diffusion-limited growth[e.g.13,21] on the one hand and adsorption-limited growth[e.g.83] on the other hand. Furthermore, it can be concluded that adsorption of large pre-ordered aggregates from solution is of utmost importance particularly in the beginning of the growth process. This is an important prerequisite for fast growth of ordered islands characteristic for sub-monolayer self-assembly films. If such pre-ordered aggregates

are not available in solution, ordered monolayers can still be obtained by adsorption of individual molecules as long as a critical temperature, which depends on the experimental conditions, is not yet reached[61]. However, in this case homogeneous growth (no islands) with significantly lower growth rates is observed. Finally, the results show that the ordering kinetics in solution leading to large aggregates is also governed by the interplay of water concentration and deposition temperature.

The ordering reactions in the deposition solution forming inverse micelles of OTS molecules surrounding small water droplets are most probably due to Van der Waals bondings without noteworthy contributions of chemical bonds, leading to loosely linked aggregates that can easily be destroyed even by shaking of the vessel.

Summarizing, it can be concluded, that deposition and growth mechanisms of octadecylsiloxane films on silicon are widely affected by ordering processes in the deposition solution prior to the immersion of the wafer. These processes are strongly influenced by the temperature and the water concentration in the solution, whereby a decreasing water concentration requires a likewise decreased temperature to yield in similar results in the subsequent deposition experiment. These ordering processes and therefore the adsorption of larger aggregates onto the surface are particularly important in the early stages of the deposition. Once these aggregates in solution get too large to fit on the residual space of the surface due to the increasing surface coverage, growth up to a full monolayer proceeds via distinctly slower adsorption of smaller aggregates or even individual molecules. In this later stage of the growth process adsorption rates decrease and surface diffusion becomes dominant.

Concluding, it has to be kept in mind that several other parameters like the substrate type or condition, the type and concentration of the precursor, and the maturation time of the solvent were held constant during all experiments in this work. It should be stressed, however, that changes of the substrate type or the precursor type leads to strongly differing growth mechanisms. Thus, the innumerable possibilities of interplays between all these deposition parameters will furthermore be a highly interesting field of future research.

Especially the ever increasing potential of modern computers will be of particular importance, as computer simulations and modeling can help to contribute to the understanding in this field of highly complex chemistry.

Finally, it should be mentioned, that this work has brought up interesting questions concerning the bonding conditions in solution, the way inverse micelles of

OTS molecules approach the surface, and the reactions that lead to adsorption of small OTS aggregates from such inverse micelles. Although several groups have investigated the adsorption of lipid vesicles on hydrophilic and hydrophobic surfaces[84,85,86,87], the adsorption of micelles of alkylsilanes on silicon remains a nearly untouched field of research.

9 Index of Figures

Figure 1: Scheme of the formation of a self-assembled monolayer (SAM).

Figure 2: Scheme of tapping mode atomic force microscopy.

Figure 3: Scheme of rotating angle ellipsometer.

Figure 4: Schematic diagram of a home-built temperature control unit (thermal insulation shell not shown). Dimensions of the sample block: h/w/d = 5/17/7 cm (with thermal insulation shell: h/w/d = 6/19/11.5 cm).

Figure 5: Image processing as performed with the software package custom-developed by C. Müllner[82]: (a) raw data; (b) line flat of the line in (a) marked with (l); (c) resulting flattened image.

Figure 6: AFM-images illustrating coverage and island size determination: The images have been obtained by processing the image shown in Figure 5c, (a) determination of the coverage, and (b) determination of the island size distribution.

Figure 7: Water concentrations in toluene determined by Karl-Fischer-titration versus nominal water concentration: titrations have been performed (■) 24 and (Δ) 48 hours after doping with bidistilled water. The data points are mean values from three titrations. The solid line is the median in the diagram. For details refer to the text.

Figure 8: Relative deviations between measured water concentration in toluene and nominal value: The data points are mean values from four independent experiments. Measurements have been performed (■) 24 and (Δ) 48 hours after doping. For details refer to the text.

Figure 9: AFM images of ODS on silicon illustrating the different possibilities of treatment of the wafer pieces after the deposition experiment: for sake of lucidity the treatment steps are given in Table 4.

Figure 10: AFM images of ODS on silicon demonstrating the influence of the water concentration in the solvent: T = 20°C, c(OTS) = 1 mmol/L, the adsorption solutions were matured for 10 min, adsorption time = 15 s; (a) c(H_2O) =

10.2 mmol/L; (b) $c(H_2O)$ = 12.7 mmol/L; (c) $c(H_2O)$ = 14.2 mmol/L; (d) $c(H_2O)$ = 16.9 mmol/L, image sizes: 25 x 25 µm².

Figure 11: AFM images of the growth of ODS on silicon at a temperature of 30°C: c(OTS) = 1 mmol/L, the adsorption solutions were matured for 10 min; (a) $c(H_2O)$ = 15.0 mmol/L, adsorption time = 10 s; (b) $c(H_2O)$ = 18.0 mmol/L, adsorption time = 5 s; image sizes: 5 x 5 µm².

Figure 12: Adsorption kinetics of OTS on silicon for different water concentrations: ellipsometric surface coverage vs. deposition time: c(OTS) = 1.0 mmol/L, maturation time of the precursor solution = 10 min, deposition temperature T = 28°C; water concentrations: (■) $c(H_2O)$ = 13.4 mmol/L; (●) $c(H_2O)$ = 10.4 mmol/L; (▲) $c(H_2O)$ = 7.3 mmol/L; (♦) $c(H_2O)$ = 5.2 mmol/L. The solid lines show a fit of the data according to a Langmuirian adsoprtion model.

Figure 13: AFM images of the growth of ODS on silicon at a temperature of 28°C: one of the kinetic series depicted in Figure 8, $c(H_2O)$ = 13.4 mmol/L, c(OTS) = 1 mmol/L, the adsorption solutions were matured for 10 min, adsorption times: (a) t = 20 s, (b) t = 40 s, (c) t = 60 s, (d) t = 90 s, (e) t = 300 s, (f) t = 1200 s; image sizes: 4 x 4 µm².

Figure 14: AFM image of OTS adsorption on silicon at a temperature of 28°C: $c(H_2O)$ = 5.2 mmol/L, c(OTS) = 1 mmol/L, the adsorption solutions were matured for 10 min, adsorption time = 15 min, image size: 4 x 4 µm².

Figure 15: Kinetic studies of the deposition of OTS on silicon: Ellipsometric surface coverages versus deposition time; $c(H_2O)$ = 13.1 mmol/L, c(OTS) = 1.0 mmol/L, maturation time of the precursor solution = 10 min; (■) T = 20°C; (○) T = 5°C.

Figure 16: AFM images of the growth of ODS on silicon: $c(H_2O)$ = 13.1 mmol/L, c(OTS) = 1.0 mmol/L, maturation time of the precursor solution = 10 min, deposition temperatures T and deposition times t: (a) T = 20°C, t = 5 s; (b) T = 20°C, t = 15 s; (c) T = 20°C, t = 30 s; (d) T = 5°C, t = 5 s; (e) T = 5°C, t = 15 s; (f) T = 5°C, t = 30 s; image sizes: (a), (b), (d) – (f) 20 x 20 µm², (c) 4 x 4 µm².

Figure 17: Ellipsometric surface coverage versus deposition temperature: c(OTS) = 1.0 mmol/L, $c(H_2O)$ = 10 mmol/L, maturation time of the precursor solution = 10 min, adsorption times are (■) t = 60 s, (▲) t = 30 s, and (●) t = 18 s.

Figure 18: AFM images of the growth of ODS on silicon: c(H_2O) = 10 mmol/L, c(OTS) = 1.0 mmol/L, maturation time of the precursor solution = 10 min, deposition temperature = 10°C, deposition times are (a), (b) t = 18 s; (c), (d) t = 60 s; image sizes: (a), (c) 25 x 25 µm²; (b), (d) 5 x 5 µm².

Figure 19: Ellipsometric surface coverage versus deposition temperature: c(OTS) = 1.0 mmol/L, c(H_2O) = 12 mmol/L, maturation time of the precursor solution = 10 min, adsorption time = 15 s. Each data point represents the mean of four individual wafers.

Figure 20: Comparison of surface coverages obtained from ellipsometry (■) and AFM (○): c(OTS) = 1.0 mmol/L, c(H_2O) = 12.0 mmol/L, maturation time of the precursor solution = 10 min, adsorption time = 15 s.

Figure 21: AFM images of OTS adsorption on silicon demonstrating the reasons for fit and misfit between AFM- and ellipsometric coverages: c(OTS) = 1.0 mmol/L, c(H_2O) = 12 mmol/L, maturation time of the precursor solution = 10 min, deposition time = 15 s; deposition temperatures, AFM-, and ellipsometric coverage: (a) T = 5°C, AFM: 62.6%, ell.: 51.0%; (b) T = 15°C, AFM: 58.6%, ell.: 60.2%; (c) T = 20°C, AFM: 43.6%, ell.: 46.1%; (d) T = 30°C; AFM: 2.2%, ell.: 14.2%; image sizes: 5 x 5 µm².

Figure 22: AFM images of OTS adsorption on silicon with very similar surface coverages as measured with ellipsometry: coverages determined by AFM data evaluation differ widely: (a) $coverage_{Ellipsometry}$ = 56.6%, $coverage_{AFM}$ = 55.7%; (b) $coverage_{Ellipsometry}$ = 53.5%, $coverage_{AFM}$ < 1%.

Figure 23: Comparison of surface coverages obtained from ellipsometry (■) and AFM (○): c(OTS) = 1.0 mmol/L, c(H_2O) = 15.0 mmol/L, maturation time of the precursor solution = 10 min, adsorption time = 10 s.

Figure 24: AFM images of a series of adsorption experiments carried out at a water content of 15 mmol/L: image sizes: (a) – (g) 25 x 25 µm², (h) 5 x 5 µm²; c(OTS) = 1.0 mmol/L, maturation time of the precursor solution = 10 min, deposition time = 10 s; deposition temperatures are (a) 10°C, (b) 17°C, (c) 19°C, (d) 21°C, (e) 23°C, (f) 25°C, (g) 27°C, (h) 30°C.

Figure 25: Island sizes as a function of the temperature as determined from AFM images: c(OTS) = 1.0 mmol/L, c(H_2O) = 15.0 mmol/L, maturation time of the precursor solution = 10 min, deposition time = 10 s.

Figure 26: The influence of agitation of the reaction vessels: mean island sizes (▲) obtained from deposition of OTS on silicon; c(OTS) = 1.0 mmol/L, $c(H_2O)$ = 15.0 mmol/L, maturation time of the precursor solution = 10 min, deposition time = 10 s, deposition temperature = 20°C; the surface coverages were obtained from ellipsometry (■) and AFM data evaluation (○).

Figure 27: Island size distributions of ODS on silicon: Influence of the agitation of the reaction vessels: c(OTS) = 1.0 mmol/L, $c(H_2O)$ = 15.0 mmol/L, maturation time of the precursor solution = 10 min, deposition time = 10 s; deposition temperatures: (a) and (b) 17°C, (c) and (d) 19°C, (e) and (f) 21°C; time between agitation and adsorption: (a), (c), and (e) 1.5 min (b), (d), and (f) 2.5 min; image sizes: 25 x 25 μm^2.

Figure 28: AFM images of ODS on silicon adsorbed at a temperature of 10°C: c(OTS) = 1.0 mmol/L, $c(H_2O)$ = 15 mmol/L, maturation time = 10 min. (a) Besides large fractally shaped islands smaller dot-like features can be observed. Image size: 5 x 5 μm^2. (b) Zoom of the lower left region in (a) showing isolated dots between the typical large islands. Image size: 1 x 1 μm^2. (c) Zoom of the upper right region in (a) showing dot-like features at different states of integration into the larger islands. Image size: 2 x 2 μm^2.

Figure 29: AFM images of ODS on silicon adsorbed at a temperature of (a) 5°C and (b) 10°C: at 5°C it can clearly be seen that the larger islands are made up by coalescence of smaller dots; c(OTS) = 1.0 mmol/L, maturation time = 10 min, $c(H_2O)$ = 12 mmol/L, deposition time = 15 s, Image sizes: 5 x 5 μm^2.

Figure 30: AFM images of the growth of ODS on silicon: c(OTS) = 1 mmol/L; the adsorption solution was matured for 10 min; (a) temperature = 13.5°C, $c(H_2O)$ = 12 mmol/L, adsorption time = 15 s; (b) temperature = 28°C, $c(H_2O)$ = 18 mmol/L, adsorption time = 5 s; image sizes: 5 x 5 μm^2.

Figure 31: Temperature of maximum surface coverage versus water concentration in the deposition solution: c(OTS) = 1 mmol/L, the maturation time of the precursor solution was 10 min in all cases, water concentrations and corresponding adsorption times: $c(H_2O)$ = 8 mmol/L, adsorption time = 30 s; $c(H_2O)$ = 10 mmol/L, adsorption time = 30 s; $c(H_2O)$ = 12 mmol/L,

adsorption time = 15 s; c(H_2O) = 15 mmol/L, adsorption time = 10 s; c(H_2O) = 18 mmol/L, adsorption time = 5 s.

Figure 32: Concentration of ordered aggregates in the precursor solution versus temperature: It should be noted that the data are depicted in form of the normalized raw signal of dynamic light scattering and that in all cases a unimodal size distribution with a constant hydrodynamic radius of 200 nm is observed. Quantification in terms of the absolute volume concentration of aggregates is not possible. c(OTS) = 1.0 mmol/L. (a) c(H_2O) = 15.0 mmol/L, the total time interval both for the cooling and the heating run was 1.5 h. (b) c(H_2O) = 12.0 mmol/L, the time interval for the heating run was 1 h.

Figure 33: Comparison of ellipsometric surface coverage (■), island size from AFM images (dotted line, Δ), and aggregate size in the precursor solution as obtained from dynamic light scattering (cooling run: solid line, heating run: dashed line): For sake of clarity DLS data are shown as modeled curves instead of individual data points. c(OTS) = 1.0 mmol/L, c(H_2O) = 15.0 mmol/L. For the adsorption experiments (i.e. island sizes and surface coverages) the maturation time of the precursor solution and adsorption time were 10 min and 10 s, respectively.

10 Index of Tables

Table 1: List of Abbreviations.

Table 2: List of chemicals used for this work.

Table 3: Solubility of H_2O in toluene at various temperatures.

Table 4: Steps of treatment leading to AFM images shown in Figure 9.

Table 5: Combination of growth parameters leading to surface coverages of approximately 60%.

Table 6: Deposition conditions and resulting mean island sizes for the wafers shown in Figure 27.

11 References

[1] Forrest, S. R. *Chem. Rev.* **1997**, 97, 1793.

[2] Chaki, N. K.; Vijayamohanan, K. *Biosens. Bioelectron.* **2002**, 17, 1.

[3] Hench, L. L. *Biomaterials: An Interfacial Approach* (Academic, New York, **1982**).

[4] Boussad, S.; Tao, N. J. *J. Am. Chem. Soc.* **1999**, 121, 4510.

[5] Perrin, A.; Lanet, V.; Theretz, A. *Langmuir* **1997**, 13, 2557.

[6] Schwartzman, M.; Sidorov, V.; Ritter, D.; Paz, Y. *J. Vac Sci. Technol. B* **2003**, 1, 148.

[7] Haneda, R.; Aramaki, K. *J. Electrochem. Soc.* **1998**, 145, 1856.

[8] Bowden, F. P.; Tabor, D. *The Friction and Lubrication of Solids* (Clarendon Press, Oxford, **1986**).

[9] Ruths, M.; Alcantar, N. A.; Israelachvili, J. N. *J. Phys. Chem. B* **2003**, 107, 11149.

[10] Amro, N. A.; Xu, S.; Liu, G.-Y. *Langmuir* **2000**, 16, 3006.

[11] Rill, Ch. *Diploma Thesis*, Vienna University of Technology **2004**.

[12] Allara, D. L.; Nuzzo, R. G. *Langmuir* **1985**, 1, 52.

[13] Woodward, J. T.; Doudevski, I.; Sikes, H. D.; Schwartz, D. K. *J. Phys. Chem. B* **1997**, 101, 7535.

[14] Wirde, M.; Gelius, U. *Langmuir* **1999**, 15, 6370.

[15] Linford, M. R.; Chidsey, C. E. D. *J. Am. Chem. Soc.* **1993**, 115, 12631.

[16] Kluth, J. G.; Sander, M.; Sung, M. M.; Maboudian, R. *J. Vac. Sci. Technol. A.* **1998** 16, 932.

[17] Ulman, A. *An introduction to ultrathin organic films: from Langmuir-Blodgett to self-assembly* (Academic Press, Boston, **1991**).

[18] Maoz, R.; Sagiv, J. *J. Colloid Interface Sci.* **1984,** 100, 465.

[19] Ulman, A. *Chem. Rev.* **1996,** 96, 1533.

[20] Schreiber, F. *Progr. Surf. Sci.* **2000,** 65, 151.

[21] Schwartz, D. K.; Steinberg, S.; Israelachvili, J.; Zasadzinski, J. A. N. *Phys. Rev. Lett.* **1992**, 69, 3354.

[22] Tidswell, I. M.; Ocko, B. M.; Pershan, P. S. *Phys. Rev. B* **1990** 41, 1111.

[23] Pomerantz, M.; Segmüller, A.; Netzer, L.; Sagiv, J. *Thin Solid Films* **1985** 132, 153.

[24] Wasserman, S. R.; Whitesides, G. M.; Tidswell, I. M.; Ocko, B. M.; Pershan, P. S.; Axe, J. D. *J. Am. Chem. Soc.* **1989**, 111, 5852.

[25] Wasserman, S. R.; Tao, Y.-T.; Whitesides, G. M. *Langmuir* **1989**, 5, 1074.

[26] Calistri-Yeh, M.; Kramer, E. J.; Sharma, R.; Zhao, W.; Rafailovich, M. H.; Sokolov, J.; Brock, J. D. *Langmuir* **1996**, 12, 2747.

[27] Banga, R.; Yarwood, J.; Morgan, A. M. *Langmuir* **1995**, 11, 4393.

[28] Barrat, A.; Silberzan, P.; Bourdieu, L.; Chatenay, D. *Europhysics Letters* **1992**, 20, 633.

[29] Britt, D.W.; Hlady, V. *J. Coll. Inter. Sci.* **1996**, 178, 775.

[30] Nakagawa, T.; Ogawa, K.; Kurumizawa, T. *Langmuir* **1994**, 10, 525.

[31] Komeda, T.; Namba, K.; Nishioka, Y. *Appl. Phys. Lett.* **1997**, 70, 3398.

[32] Komeda, T.; Namba, K.; Nishioka, Y. *J. Vac. Sci.* Technol. A. **1998**, 16, 1680.

[33] Vallant, T.; Kattner, J.; Brunner, H.; Mayer, U.; Hoffmann, H. *Langmuir* **1999,** 15, 5339.

[34] Banga, R.; Yarwood, J.; Morgan, A. M. *Langmuir* **1995**, 11, 618.

[35] Tidswell, I. M.; Rabedeau, T. A.; Pershan, P. S.; Kosowsky, S. D. *J. Chem. Phys.* **1991**, 95, 2854.

[36] Ye, S.; Nihonyanagi, S.; Uosaki, K. *Phys. Chem. Chem. Phys.* **2001**, 3, 3463.

[37] Parikh, A. N.; Schivley, M. A.; Koo, E.; Aurentz, D.; Mueller, K.; Allara, D. L. *J. Am. Chem. Soc.* **1997**, 119, 3135.

[38] Ho, M.; Pemberton, J.E. *Anal. Chem.* **1998**, 70, 4915.

[39] Kluth, G. J.; Carraro, C.; Maboudian, R. *Phys. Rev. B.* **1999**, 59, R10449

[40] Vilar, M. R.; Bouali, Y.; Kitakatsu, N.; Lang, Ph., Michalitsch, R.; Garnier, F.; Dubot, P. *Thin Solid Films* **1998**, 327-329, 236.

[41] Houssiau, L.; Bertrand, P. *Appl. Surf. Sci.* **2001**, 175-176, 351.

[42] Wolf, K. V.; Cole, D. A.; Bernasek, S. L. *Anal. Chem.* **2003**, 74, 5009.

[43] Resch, R.; Grasserbauer, M.; Friedbacher, G.; Vallant, T.; Brunner, H.; Mayer, U.; Hoffmann, H. *Appl. Surf. Sci.* **1999**, 140, 168.

[44] Leitner, T.; Friedbacher, G.; Vallant, T.; Brunner, H.; Mayer, U.; Hoffmann, H. *Mikrochim. Acta* **2000**, 133, 331.

[45] Brunner, H.; Vallant, T.; Mayer, U.; Hoffmann, H.; Basnar, B.; Vallant, M.; Friedbacher, G. *Langmuir* **1999,** 15, 1899.

[46] Terrill, R. H.; Tanzer, T. A.; Bohn, P. W. *Langmuir,* **1998,** 14, 845.

[47] Foisner, J.; Glaser, A.; Kattner, J.; Hoffmann, H.; Friedbacher, G. *Langmuir* **2003,** 19, 3741.

[48] Foisner, J: *Dissertation*, Vienna University of Technology, Austria, **2003**.

[49] Rozlosnik, N.; Gerstenberg, M. C.; Larsen, N. B. *Langmuir,* **2003,** 19, 1182.

[50] Allara, D. L.; Parikh, A. N.; Rondelez, F. *Langmuir* **1995,** 11, 2357.

[51] Iimura, K.-I.; Nakajima, Y.; Kato, T. *Thin Solid Films* **2000**, 379, 230.

[52] Angst, D. L.; Simmons, G. W. *Langmuir* **1991,** 7, 2236.

[53] Bierbaum, K.; Grunze, M.; Baski, A. A.; Chi, L. F.; Schrepp, W.; Fuchs, H. *Langmuir* **1995**, 11, 2143.

[54] Lio, A.; Charych, D. H.; Salmeron, M. *J. Phys. Chem. B* **1997,** 101, 3800.

[55] Vallant, T.; Brunner, H.; Mayer, U.; Hoffmann, H.; Leitner, T.; Resch, R.; Friedbacher, G. *J. Phys. Chem. B* **1998**, 102, 7190.

[56] Le Grange, J. D.; Markham, J. L.; Kurkjian, C. R. *Langmuir* **1993,** 9, 1749.

[57] Barrer, R. M. *Zeolites and Clay Minerals as Sorbents and Molecular Sieves*; (Academic Press, London), **1978**.

[58] Rye, R. R.; Nelson, G. C.; Dugger, M. T. *Langmuir* **1997**, 13, 2965.

[59] Bunker, B. C.; Carpick, R. W.; Assink, R. A.; Thomas, M. L.; Hankins, M. G.; Voigt, J. A.; Sipola, D.; de Boer, M. P.; Gulley, G. L. *Langmuir* **2000**, 16, 7742.

[60] Brzoska, J. B.; Shahidzadeh, N.; Rondelez, F. *Nature* **1992**, 360, 719.

[61] Parikh, A. N.; Allara, D. L.; Azuz, I. B.; Rondelez, F. *J. Phys. Chem.* **1994**, 98, 7577.

[62] Rye, R. R. *Langmuir* **1997**, 13, 2588.

[63] Carraro, C.; Yauw, O. W.; Sung, M. M.; Maboudian, R. *J. Phys. Chem. B* **1998**, 102 (23), 4441.

[64] Zhao, X.; Kopelman, R.; *J. Phys. Chem.* **1996**, 100, 11014.

[65] Silberzan, P.; Léger, L.; Ausserré, D.; Benattar, J. J. *Langmuir* **1991**, 7, 1647.

[66] Tripp, C. P.; Hair, M. L. *Langmuir* **1995**, 11, 1215.

[67] Chen, L.-J.; Tsai, Y.-H.; Liu, C.-S.; Chiou, D.-R.; Yeh, M.-C. *Chem. Phys. Letters* **2001**, 346, 241.

[68] Binnig, G.; Rohrer, H.; Gerber, C.; Weibel, E. *Applied Physics Letters* **1982**, *49*, 57.

[69] Binnig, G.; Quate, C.; Gerber, C. *Physical Review Letters* **1986**, *56*, 930.

[70] Schmitz, I. *Dissertation*, Vienna University of Technology **1996**.

[71] Leitner, T. *Diploma Thesis*, Vienna University of Technology **1998**.

[72] McCrackin, F.; Passaglia, E.; Stromberg, R.; Steinberg, H. *J. Res. Natl. Bur. Stand. Sect. A* **1963**, 67, 363.

[73] Palik, E. D. *Handbook of Optical Constants of Solids*, Academic, New York, **1985**.

[74] Sohar, Ch. R. *Diploma Thesis*, Vienna University of Technology **2005**.

[75] Berne, B. J.; Pecora R. *Dynamic Light Scattering*, Dover Publication Inc, New York **2000**, 3.

[76] Dörfler, H.-D. *Grenzflächen und kolloid-disperse System: Physik und Chemie*, Springer-Verlag: Berlin - Heidelberg - New York **2002,** 687.

[77] Glasoe, P. K.; Schultz S. D. *J. Chem. Eng. Data* **1972**, 17, 66.

[78] Rosenbaum, C. K.; Walton, J. H. *J. Am. Chem. Soc.* **1930**, 52, 3568.

[79] Tarasenkov, D. N.; Polozhintzeva, E. N. *Ber.* **1932**, 65B, 184.

[80] Johnson, J. R.; Christian, S. D.; Affsprung, H. E. *J. Am. Chem. Soc. A* **1966**, 77.

[81] Scholz, E. *Karl-Fischer-Titration*, Springer-Verlag, Berlin, **1984**.

[82] Müllner, C. *Diploma Thesis*, Vienna University of Technology **2003**.

[83] Cheng, S. S.; Scherson, D. A.; Sukenik, C. N. *J. Am. Chem. Soc.* **1992**, 114, 5436.

[84] Williams, L. M.; Evans, S. D.; Flynn, T. M.; Marsh, A.; Knowles, P. F.; Bushby, R. J.; Boden, N. *Langmuir* **1997,** *13,* 751.

[85] Lingler, S.; Rubinstein, I.; Knoll, W.; Offenhäusser, A. *Langmuir* **1997,** *13,* 7085.

[86] Nissen, J.; Gritsch, S.; Wiegand, G.; Rädler, J.O. *Eur. Phys. J. B* **1999**, 10, 335.

[87] Jenkins, A. T. A.; Bushby, R. J.; Evans, S. D.; Knoll, W.; Offenhäusser, A.; Ogier, S. D. *Langmuir* **2002,** *18,* 3176.

Lebenslauf

Persönliche Daten:	
Name:	DI Andreas Glaser
Anschrift:	Sonnleithnergasse 57/3/26, A-1100 Wien
Telefon:	0699/11751286 bzw. 01/2642314
e-Mail:	andreas.glaser@tuwien.ac.at
Geburtsdatum:	25. April 1974
Geburtsort:	Wien
Familienstand:	Lebensgemeinschaft
Staatsbürgerschaft:	Österreich
Schulbildung:	
1980-1992	Volksschule der Stadt Wien, Karl Löwe-Gasse 20, 1120 Wien Naturwissenschaftl. Realgymnasium, BRG Wien V, Reinprechtsdorferstraße 24, 1050 Wien
Mai 1992	Matura mit ausgezeichnetem Erfolg
Studium:	
1992-2001	Studium der Technischen Chemie an der TU Wien, Studienzweig Analytische & Physikalische Chemie; Diplomarbeit in der Arbeitsgruppe Photochemie des Instituts

	für Materialchemie: **„Phenolbelastete Abwässer: Analytik und Abbau mit dem Photo-Fenton-Verfahren“**, Betreuer: Prof. Rupert Bauer, Abschluss mit Auszeichnung
2002-2004	Dissertation in der Arbeitsgruppe Mikro- und Nanoanalytik des Inst. F. Chemische Technologien und Analytik, Betreuer: Prof. Gernot Friedbacher
04.2005-07.2005	Fertigstellung der Dissertation **„Investigation of the Effects of Water and Temperature on the Adsorption of Alkylsiloxane Self-Assembled Monolayers on Silicon”**
Berufserfahrung:	
1992-1995	Mehrere Ferialanstellungen
2000	Anstellung bei Ao. Univ. Prof. DI Dr. Rupert Bauer, TU Wien
2002-2004	Wissenschaftlicher Mitarbeiter bei Ao. Univ. Prof. DI Dr. Gernot Friedbacher, TU Wien
2004-2005	Zivildienst in der Blutspendezentrale des Österreichischen Roten Kreuzes
08.2005-	Angestellter OMV Deutschland GmbH
Weitere Informationen:	
IT-Kenntnisse	Windows (NT, 2000, XP), Microsoft Office, Chemiesoftware (Datenbanken, Zeichenprogramme), Corel Draw, ...
Sprachkenntnisse	Deutsch: Muttersprache Englisch: verhandlungsfähig Latein: Grundkenntnisse
Führerschein	Gruppen A und B
Hobbys	Leichtathletik, Handball, Rollenspielen, Darts, Skifahren,...